

UNCLASSIFIED

SECRET

MAR 20 1952

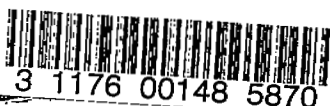
Copy  
RM L50L19

9

NACA RM L50L19

~~CONFIDENTIAL~~

MAR 12 1951



NACA

## RESEARCH MEMORANDUM

STATIC LONGITUDINAL STABILITY AND DYNAMIC CHARACTERISTICS  
AT HIGH ANGLES OF ATTACK AND AT LOW REYNOLDS NUMBERS OF  
A MODEL OF THE X-3 SUPERSONIC RESEARCH AIRPLANE

By Sanger M. Burk, Jr., and Burton E. Hultz

Langley Aeronautical Laboratory

Langley Field, Va.

CLASSIFICATION CHANGED

~~CONFIDENTIAL~~

NACA Release

To

By authority of

Date

Feb. 28, 1952

CLASSIFIED DOCUMENT

This document contains information affecting the National Defense of the United States within the meaning of the Espionage Act, USC 50:51 and 52. Its transmission or the revelation of its contents in any manner to an unauthorized person is prohibited by law.

Information so classified may be imparted only to persons in the military and naval services of the United States, appropriate civilian officers and employees of the Federal Government who have a legitimate interest therein, and to United States citizens of known loyalty and discretion who of necessity must be informed thereof.

NATIONAL ADVISORY COMMITTEE  
FOR AERONAUTICS

WASHINGTON

February 6, 1951

NACA LIBRARY

LANGLEY AERONAUTICAL LABORATORY

Langley Field, Va.

To UNCLASSIFIED

CLASSIFICATION CHANGED

By authority of Release Form 2819

Date Oct. 29, 1954

J. H. Langley per NACA

11-4-54

~~CONFIDENTIAL~~

SECRET

NACA LIBRARY

SECURITY INFORMATION

UNCLASSIFIED

LANGLEY AERONAUTICAL LABORATORY

Langley Field, Va.

~~CONFIDENTIAL~~  
~~SECURITY INFORMATION~~

## NATIONAL ADVISORY COMMITTEE FOR AERONAUTICS

## RESEARCH MEMORANDUM

STATIC LONGITUDINAL STABILITY AND DYNAMIC CHARACTERISTICS  
AT HIGH ANGLES OF ATTACK AND AT LOW REYNOLDS NUMBERS OF  
A MODEL OF THE X-3 SUPERSONIC RESEARCH AIRPLANE

By Sanger M. Burk, Jr., and Burton E. Hultz

## S U M M A R Y

An investigation was conducted in the Langley 20-foot free-spinning tunnel to determine the motions and trim conditions possible from  $0^\circ$  to  $90^\circ$  angle of attack for the X-3 airplane which is a supersonic airplane having an extremely long nose and a small wing. Tests were conducted on both a  $\frac{1}{40}$ -scale dynamic model and a  $\frac{1}{10}$ -scale static model at low Reynolds numbers. Force tests on the component parts of the static model were included in the investigation. Tests were also conducted in the Langley 300 MPH 7- by 10-foot tunnel on the complete static model at somewhat higher Reynolds numbers.

Results obtained in the Langley 20-foot free-spinning tunnel on both the dynamic and static models indicated unsatisfactory pitching-moment characteristics at high angles of attack in that the models showed a trim condition at these high angles of attack; deflecting the horizontal tail had negligible effect on changing this trim condition. There was a slight indication of scale effect, however, for the force tests conducted in the spin tunnel for Reynolds numbers varying from approximately 130,000 to 413,000. Tests were conducted, therefore, in the Langley 300 MPH 7- by 10-foot tunnel at a Reynolds number slightly in excess of 1,000,000. Based on the static pitching-moment characteristics alone, the results indicated that a corresponding airplane at low-subsonic Mach numbers probably would not have a high-angle-of-attack trim condition; however, calculations indicated that at high-subsonic Mach numbers it might be possible for the airplane to trim at high angles of attack. There was no appreciable scale effect indicated on the pitching-moment coefficients at low angles of attack.

~~CONFIDENTIAL~~  
~~SECURITY INFORMATION~~

The results of the investigation, in general, indicate that scale effect may appreciably influence free dynamic results obtained at low Reynolds numbers and high angles of attack on a design having a very long nose and a very small wing.

## INTRODUCTION

During an investigation to determine the spin and recovery characteristics of a dynamic model representative of a supersonic airplane having an extremely long nose and a small wing, unusual motions accompanied by a longitudinal trim condition at extremely high angles of attack were observed. In order that the results being obtained from the dynamic model could be better understood and evaluated a static model was built for test on the six-component balance in the Langley 20-foot free-spinning tunnel. Force tests were performed on the complete static model and also on its component parts. The Reynolds number range of the force tests in the spin tunnel varied from approximately 130,000 to 413,000. In order to extend the Reynolds number range, force tests were also conducted in the Langley 300 MPH 7- by 10-foot tunnel up to a Reynolds number of 1,124,000.

The present report presents the results of both the dynamic and static tests.

## SYMBOLS

The data presented herein are in the form of standard NACA coefficients of forces and moments which are referred to both the body and wind axes with their origin at the center of gravity of the model. The positive directions of the forces and moments and angular displacements are shown in figure 1. The center of gravity of the model is at the 10-percent point of the mean aerodynamic chord (see fig. 2).

$C_L$	lift coefficient—(Lift/ $qS$ )
$C_D$	drag coefficient (Drag/ $qS$ )
$C_Z$	normal-force coefficient (Normal force/ $qS$ )
$C_X$	longitudinal-force coefficient (Longitudinal force/ $qS$ )
$C_m$	pitching-moment coefficient (Pitching moment/ $qS\bar{c}$ )
$q$	free-stream dynamic pressure, pounds per square foot $\left(\frac{\rho V^2}{2}\right)$

~~CONFIDENTIAL~~  
SECURITY INFORMATION

NACA RM L50L19

3

$\rho$	mass density of air, slugs per cubic foot
$V$	free-stream velocity, feet per second
$M$	free-stream Mach number
$S$	wing area, square feet
$\bar{c}$	mean aerodynamic chord, $\frac{2}{S} \int_0^{b/2} c^2 dy$ where $c$ is local chord and $y$ is spanwise ordinate, feet
$b$	wing span, feet
$\alpha$	angle of attack of the fuselage reference line with respect to wind axis, degrees
$R$	Reynolds number based on mean aerodynamic chord of wing
$R_{\text{fuselage}}$	Reynolds number based on maximum depth of the fuselage
$\delta_t$	deflection of all-movable horizontal tail with respect to fuselage reference line, positive with trailing edge downward, degrees
$\delta_r$	rudder deflection with respect to fin, positive with trailing edge to left, degrees
$\delta_{f_n}$	leading-edge-flap deflection, positive downward, degrees
$\delta_f$	trailing-edge-flap deflection, positive downward, degrees
$m$	mass of airplane, slugs
$I_X, I_Y, I_Z$	moments of inertia about X, Y, and Z body axes, respectively, slug-feet <sup>2</sup>
$\frac{I_X - I_Y}{mb^2}$	inertia yawing-moment parameter
$\frac{I_Y - I_Z}{mb^2}$	inertia rolling-moment parameter
$\frac{I_Z - I_X}{mb^2}$	inertia pitching-moment parameter

~~CONFIDENTIAL~~  
SECURITY INFORMATION

~~CONFIDENTIAL~~  
SECURITY INFORMATION

4

NACA RM L50L19

$\mu$  airplane relative density ( $m/\rho S b$ )  
 $\partial C_m / \partial \alpha$  rate of change of pitching-moment coefficient with angle of attack, per degree

A P P A R A T U S A N D M E T H O D S

MODEL

A small dynamic model and a larger static model of the X-3 supersonic research airplane were constructed at the Langley Laboratory of the NACA. The scale of the dynamic model was 1/40, and the scale of the larger static model was 1/10. The fuselage of the dynamic model was made principally of balsa, the wing was made of dural, and the vertical and horizontal tails were made of steel. The fuselage of the static model consisted primarily of a plywood hull planked with balsa; the wing and the vertical and horizontal tails were made of laminated mahogany. The design had low-aspect-ratio wing and tail surfaces and incorporated an all-movable horizontal tail. The wing of the design was relatively small when compared to the size of the fuselage. The airscops of the design were not ducted. A three-view drawing of the  $\frac{1}{10}$ -scale static model is shown on figure 2. A photograph showing the two models is presented as figure 3. The dimensional characteristics of the airplane are given in table I.

WIND TUNNELS

The Langley 20-foot free-spinning tunnel used for most of the tests is a vertical wind tunnel of dodecagonal cross section and is capable of airspeeds up to approximately 60 miles per hour.

The Langley 300 MPH 7- by 10-foot tunnel used for some of the tests is a horizontal atmospheric closed tunnel of the return-flow type.

TESTING TECHNIQUE

In order to study and evaluate the motions and longitudinal trim characteristics of the models, four different testing techniques were used and are described in the following paragraphs.

~~CONFIDENTIAL~~  
SECURITY INFORMATION

#### Free-Rotation Tests

For the free-rotation tests, the same technique as used for spin tests was generally used, that is, the model was launched by hand with spinning rotation into the vertically rising air stream which was adjusted until the force of the rising air stream balanced the weight of the model. Visual observations and motion-picture records were made then of the motion exhibited by the model.

#### Glide Tests

Glide tests were performed with the dynamic model by clamping the model in a special rig fixed in the center of the spin tunnel (see fig. 4) and releasing the model at various known angles of attack and horizontal tail deflections and observing its path and motion.

#### Trim-Rig Tests

For a few tests the dynamic model was mounted at its center of gravity on a rig resembling a yoke (fig. 5) in such a manner that the model had only one degree of freedom which was freedom to pitch about the Y-axis. At the test airspeed, the model was displaced from its normal trimmed position by an extraneous force so that the angle of attack ranged through approximately  $\pm 90^\circ$ . It was then freed to assume a trim attitude. The trim attitude was recorded by photographs.

#### Balance Tests

The force and moment data were obtained in the spin tunnel by mounting the static model on a six-component strain-gage balance which measures the data about the body axes. Reference 1 gives a detailed description of the balance. The static model is shown mounted on the balance in the spin tunnel in figure 3. The balance is shown in detail in figure 6.

In the Langley 300 MPH 7- by 10-foot tunnel the static model was mounted on a balance system that measured forces and moments about the wind axes. The static model mounted in the Langley 300 MPH 7- by 10-foot tunnel is shown as figure 7.

TEST CONDITIONS

DYNAMIC TESTS

The free-rotation, glide, and trim-rig tests were performed with the dynamic model in the clean condition except for a few tests with the flaps deflected. The mass conditions and inertia parameters for the loadings tested on the model (converted to full-scale values) are listed in table II. The test Reynolds number of the dynamic model based on the mean aerodynamic chord was approximately 85,000. This value was not corrected for the turbulence factor of the spin tunnel which is approximately 1.8.

The control deflections used in the tests were:

Rudder, degrees . . . . .	20, 0, -20
Horizontal tail, degrees . . . . .	10, 0, $-2\frac{1}{2}$ , -5, -10, -15, -25
Ailerons, degrees . . . . .	12, 0, -12

For the free-rotation tests in addition to the control settings mentioned previously the leading-edge flaps were deflected  $30^\circ$  down for some of the tests and the trailing-edge flaps were deflected  $50^\circ$  down independently and in combination with the leading-edge flaps. For the glide tests the rudder and ailerons were set at neutral while the horizontal tail was set at various deflections and the model was released through a range of angles of attack from  $-20^\circ$  to  $90^\circ$ . For the trim-rig tests the rudder and ailerons were set at neutral and the horizontal tail set at various deflections.

STATIC TESTS

As previously mentioned, balance tests in the spin tunnel were conducted with the static model and its component parts. The fuselage-alone component of the model included the vertical tail. The angle of attack was varied from  $0^\circ$  to  $90^\circ$  at  $0^\circ$  yaw. The rudder and ailerons were set at neutral and the horizontal tail was set at various deflections. The leading- and trailing-edge flaps were deflected  $30^\circ$  and  $50^\circ$ , respectively, for a few tests. Tests were conducted for a range of dynamic pressures from approximately 0.8 to 8.0 pounds per square foot and the corresponding Reynolds numbers, based on the mean aerodynamic chord of the static model, ranged from 130,000 to 413,000. This was the maximum range of Reynolds number possible in the tunnel for this model. These values of Reynolds numbers have not been corrected for the turbulence factor of the spin tunnel.

~~CONFIDENTIAL~~  
SECURITY INFORMATION

NACA RM L50L19

7

Balance tests in the Langley 300 MPH 7- by 10-foot tunnel were conducted on the static model generally from  $0^\circ$  to  $90^\circ$  angle of attack at  $0^\circ$  yaw. The horizontal tail, as previously mentioned, was set at various deflections while the ailerons and rudder were set at neutral. The tests were performed at dynamic pressures ranging from 5.0 to 60.0 pounds per square foot and the corresponding Reynolds numbers, based on the mean aerodynamic chord of the model, ranged from 325,000 to 1,124,000. These values of Reynolds numbers have not been corrected for the turbulence factor of the tunnel, which is not known but thought to be small because of the fairly high contraction ratio of the tunnel.

A C C U R A C Y

DYNAMIC TESTS

The dynamic-model test results presented herein are believed to be the true values given by the model within the following limits:

$\alpha$ , degrees . . . . .	$\pm 1$
V, percent . . . . .	$\pm 5$

The limits of accuracy of the measurements of the mass characteristics of the dynamic model are believed to be as follows:

Weight, percent . . . . .	$\pm 1$
Center-of-gravity, percent $\bar{c}$ . . . . .	$\pm 1$
Moments of inertia, percent . . . . .	$\pm 5$

The controls were set with an accuracy of  $\pm 1^\circ$ .

S T A T I C   T E S T S

The limits of accuracy in setting the angle of attack and free-stream velocity are believed to be as follows:

$\alpha$ , degrees . . . . .	$\pm 0.5$
V, percent . . . . .	$\pm 1.5$

The tunnel-wall effects on the static model were not considered significant for the spin-tunnel tests since the model was located an appreciable distance from the tunnel wall and was small with relation to the tunnel diameter. The model normally was pivoted at the end of a horizontal arm (fig. 6) and at large angles of attack as the model

~~CONFIDENTIAL~~  
SECURITY INFORMATION



approached the horizontal position the fuselage came very close to the arm. To determine the possible interference effect of the horizontal arm, a slender streamline strut approximately  $1\frac{1}{2}$  feet in length was mounted at the center of gravity of the model parallel to the Z body axis while the other end of the strut was attached to the end of the horizontal arm. Thus the model would remain displaced  $1\frac{1}{2}$  feet away from the horizontal arm for all angles of attack. No appreciable difference between the results was noted when testing with and without the strut.

Jet boundary corrections were not applied to results obtained in the Langley 300 MPH 7- by 10-foot tunnel because the corrections were considered negligible since the size of the model was considered small relative to the size of the tunnel. Blocking effects were also considered negligible because of the low tunnel airspeed and the relatively small size of the model. The data for Reynolds number values of 325,000 and 562,000 obtained in the Langley 7- by 10-foot tunnel were somewhat erratic because the small size of the model in the Langley 7- by 10-foot tunnel and the relatively low airspeeds of the tests resulted in force and moment values smaller than those that could be accurately measured on the balance.

#### P R E S E N T A T I O N O F R E S U L T S

Film strips showing various motions of the dynamic model possible after it has been launched into the spin tunnel are presented in figure 8. The results of the free-rotation tests are presented on charts 1 to 7. The order used for presenting the data on the charts is as follows: horizontal rows from top to bottom present the results obtained with the horizontal tail deflected full up (stick full back), neutral, and full down, respectively. Vertical columns from left to right present results obtained with the ailerons deflected full against (stick full left for right rotation), neutral, and full with the rotation, respectively. The results of the glide tests and of the trim rig tests are presented on tables III and IV, respectively. The results of the static-model tests for six horizontal tail deflections at a Reynolds number of 340,000 is shown in figure 9. The effect of flap deflection is shown in figure 10. The results of the static-model tests in the spin tunnel for various Reynolds numbers and with the horizontal tail set at  $0^\circ$  is shown in figure 11. The results of the static-model tests in the Langley 7- by 10-foot tunnel for various Reynolds numbers and three horizontal tail deflections is shown in figures 12 and 13. Figure 14 presents the results of tests of the fuselage alone for various Reynolds numbers. A comparison between experimental and calculated results for the fuselage-alone condition at a relatively low and at relatively high Reynolds

number is shown in figure 15. The results of tests of the wing alone, the fuselage plus wing, and the fuselage plus horizontal tail for various Reynolds numbers are shown in figures 16, 17, and 18, respectively.

## DISCUSSION OF RESULTS

### DYNAMIC TESTS

#### Free-Rotation Tests

The results of routine spin tests of the dynamic model in general indicated that the model tended to trim at high angles of attack with some pitching oscillations (average  $\alpha$  approximately  $70^\circ$  to  $75^\circ$ ) for all horizontal tail deflections. Charts 1 to 7 present these results in detail. Briefly, one of the following motions was generally obtained during the free-rotation tests, these motions generally accompanying the tendency of the model to trim at high angles of attack: The launching rotation ceased and the model glided, oscillating approximately  $\pm 15^\circ$  in roll (fig. 8(a)); the launching rotation ceased and the model rolled rapidly about its X body axis (fig. 8(b)); the launching rotation decreased until the model rotated slowly at a constant rate about a vertical axis in a wide stalled gliding turn while oscillating approximately  $\pm 15^\circ$  in roll (fig. 8(c)); or the launching rotation increased until the model rotated at a very rapid rate about its Z body axis (fig. 8(d)). Another interesting motion which sometimes occurred was one in which the model continued to rotate moderately about a vertical axis and at the same time rolled rapidly about its X body axis, the rotations being in the same sense and the X body axis being at approximately  $50^\circ$  from the vertical axis (fig. 8(e)). This motion was made possible apparently by the introduction of a nose-down gyroscopic moment resulting from the combined rotations of the model.

The continuous rolling motion about the X body axis, previously mentioned, apparently occurred only when the rolling moment contributed by the rudder and that contributed by the ailerons were additive. The rolling moment contributed by the rudder was relatively large because the rudder was mounted high above the fuselage center line.

The motions or trim characteristics did not appear to be affected by flap settings.

### Glide Tests

Because it was believed that the unusual trim conditions obtained during free-rotation tests may have been primarily attributable to the longitudinal characteristics of the model, glide tests were performed to evaluate the trim characteristics further.

The results of the glide tests (table III) indicate that for any upward deflection of the horizontal tail the model would pitch up and trim at approximately  $70^\circ$  angle of attack. When the horizontal tail was set at neutral and the model released at an angle of attack of  $19^\circ$  or greater, the model pitched up and trimmed at  $70^\circ$  angle of attack; below  $19^\circ$  angle of attack, it pitched down. When the horizontal tail was set full down and the model released at an angle of attack greater than  $26^\circ$ , the model pitched up to  $70^\circ$  angle of attack; below  $26^\circ$  angle of attack, it pitched down. It was thus apparent that any up horizontal-tail deflection would cause an upward pitching moment at any positive angle of attack below  $70^\circ$  and that at any angle of attack above  $26^\circ$  it would be impossible to reenter the normal-flight region deflecting the horizontal tail.

### Trim-Rig Tests

Before making extensive static force and moment measurements to obtain an evaluation of the unusual trim characteristics of the model, it was felt desirable to obtain a qualitative indication of whether the trim characteristics were primarily associated with dynamic or static parameters.

The results obtained on the trim rig are presented in table IV and indicate stable trim angles at high angles of attack for all horizontal tail settings. This was taken as an indication that the unusual trim characteristics of the model were primarily associated with its static pitching-moment characteristics.

### STATIC TESTS

In order to afford a better understanding of the results obtained on the dynamic model, force and moment data were obtained on a static model. The data used in analyzing the static longitudinal characteristics of the model were  $C_m$  and  $C_z$ . The values of  $C_L$ ,  $C_D$ , and  $C_x$  also have been included in this paper although not discussed specifically.

Complete Model

Spin-tunnel balance tests.- The variation of the pitching-moment coefficient  $C_m$  with angle of attack  $\alpha$  for various horizontal tail settings is presented in figure 9. The data were obtained in the spin tunnel at a Reynolds number of 340,000. The data show a high-angle-of-attack trim condition varying from  $75^\circ$  to  $80^\circ$  angle of attack for all horizontal tail settings indicating the ineffectiveness of the horizontal tail as a means to trim the model back into the normal flight region once it has reached this high trim angle. The slope of the curve appears to be quite steep at the point of trim thus indicating a very stable condition. For horizontal tail settings of  $-5^\circ$  and  $0^\circ$  in addition to this trim point at very high angles of attack, alternate stable trim points at lower angles of attack were also possible as shown in figure 9. Deflecting the flaps (fig. 10) had negligible effect on changing the high-angle-of-attack trim condition although the low-angle-of-attack trim conditions were changed somewhat.

To determine possible effects of Reynolds number on the static data for this model, the balance tests in the spin tunnel were made through the widest range of airspeeds possible, corresponding, as previously indicated, to Reynolds number values of 130,000 to 413,000. The variation of the pitching-moment coefficient with angle of attack for various Reynolds numbers and with the horizontal tail set at  $0^\circ$  is presented in figure 11. Increasing the Reynolds number generally caused an appreciable reduction in the nose-up pitching moment and although the high-angle-of-attack trim was still obtained there appeared to be a definite indication that further increases in Reynolds number might lead to the elimination of the trim points.

Comparison of figures 9 and 11 for a horizontal tail setting of  $0^\circ$  and a Reynolds number of 340,000 indicates a small difference in the results. Inasmuch as the results were obtained during different test runs, the small differences may be attributed to slight variations in setting the attitudes and controls of the model.

The variation of the normal-force coefficient  $C_z$  with angle of attack  $\alpha$  for various horizontal tail settings is presented on figure 9. As would be expected, for any given angle of attack,  $C_z$  generally increased negatively (upward normal force increased) as the horizontal tail was deflected from up to down. The variation of  $C_z$  with angle of attack for various Reynolds numbers is shown on figure 11. The results indicated that there was no appreciable variation of  $C_z$  with Reynolds number from  $0^\circ$  to  $90^\circ$  angle of attack. The center of pressure, however, moved in a rearward direction towards the center of gravity as the Reynolds number was increased. The results indicate that, for the complete model, since the nose-up pitching moment was reduced and the normal

force did not change with an increase in Reynolds number, the change in stability, therefore, was a result of a redistribution of the normal force rather than a change in its magnitude.

The variation of lift coefficient with angle of attack is shown in figure 9 for the complete model. An initial stall occurred at approximately  $14^\circ$  angle of attack and a subsequent stall occurred between  $40^\circ$  and  $50^\circ$  angle of attack. Corresponding lift curves for wing alone (fig. 16) and fuselage alone (fig. 14) indicate that the initial loss in lift was due to the stalling of the wing and that the subsequent loss in lift was due to a rapid decrease in the lift of the wing beyond approximately  $50^\circ$  angle of attack and also due to the stalling of the fuselage. From examination of figures 9 and 16, it appears that due to interference effects the wing stalls earlier when in combination with the fuselage.

Langley 300 MPH 7- by 10-foot-tunnel balance tests.- In order to obtain pitching-moment characteristics at Reynolds numbers beyond those possible in the spin tunnel, tests were conducted in the Langley 300 MPH 7- by 10-foot tunnel up to a Reynolds number value of 1,124,000. In order to obtain a qualitative comparison with the spin-tunnel balance results the 7- by 10-foot-tunnel investigation included tests at lower Reynolds numbers varying down to a value of 325,000. The variation of pitching-moment coefficient with angle of attack for Reynolds numbers ranging from 325,000 to 1,124,000 is shown in figure 12. It can be seen that, when the Reynolds number was increased from a relatively low value to a high value, the slopes of the pitching-moment curves became stable from approximately  $20^\circ$  to  $90^\circ$  angle of attack. Thus the data indicate that a high-angle-of-attack trim condition will not be obtained at high Reynolds numbers (based on static  $C_m$  characteristics alone). When the horizontal tail was deflected full up, the model trimmed at approximately  $40^\circ$  angle of attack, but it appeared that the deflection of the horizontal tail down would be effective in terminating this condition (see fig. 13). Results in figures 12 and 13 also show a static longitudinal instability between approximately  $13^\circ$  and  $25^\circ$  angle of attack for all Reynolds numbers tested. This unstable region begins at the angle of attack of the initial stall of the complete model.

On the basis of static pitching-moment characteristics alone, the results indicate that large scale effects at high angles of attack may be obtained on a design incorporating an extremely long nose and small wing. A corresponding full-scale airplane at low-subsonic Mach numbers may not trim at the high angles of attack indicated by the lower scale model tests.

There was no appreciable effect of Reynolds number on  $C_m$  up to approximately  $16^\circ$  angle of attack even for the highest Reynolds number tested in the 7- by 10-foot tunnel as also previously indicated by spin-tunnel balance tests.

The balance tests on the model, although indicating a change in  $C_m$  with Reynolds number at high angles of attack, indicated no appreciable variation of  $C_Z$ ,  $C_L$ ,  $C_D$ , and  $C_X$  with Reynolds number from  $0^\circ$  to  $90^\circ$  angle of attack (see fig. 12) for the range of Reynolds numbers tested.

The data for Reynolds number values of 325,000 and 562,000 (fig. 12), although erratic because of reasons given previously, were nevertheless in qualitative agreement with corresponding spin-tunnel results.

#### Component Parts of Model

In an effort to determine why there was a large scale effect on  $C_m$  at high angles of attack for the complete model and no appreciable effect on the force coefficients, it was considered desirable to obtain balance data on component parts of the static model at various Reynolds numbers. Such tests could be conveniently made in the spin tunnel and although it was recognized that the range of Reynolds number possible (up to 413,000) was limited, nevertheless it was felt that such data would be of value in a better understanding of the results obtained on the complete model.

Fuselage alone.— The variations of  $C_m$  and  $C_Z$  with angle of attack for various Reynolds numbers for the fuselage-alone condition are presented in figure 14. The data indicate that the unstable pitching moment of the fuselage increased as the angle of attack was increased to  $60^\circ$  and then decreased as the angle of attack was increased to  $90^\circ$ . In general, for angles of attack above  $30^\circ$  the unstable pitching moment of the fuselage decreased somewhat as the Reynolds number increased. The change in  $C_m$  due to Reynolds number (130,000 to 413,000 based on the M.A.C. or 80,000 to 255,000 based on fuselage maximum depth) for the fuselage alone was of the same order of magnitude as was that of the complete model. Figure 14 shows that  $C_Z$  generally had a tendency to decrease with an increase in Reynolds number for a given angle of attack.

The results for the fuselage alone were in agreement with the results predicted in reference 2 in that these test results indicated that the scale effect on  $C_m$  was due to the decrease in drag (or  $C_Z$ ) with an increase in Reynolds number. The calculations in reference 2 were based on reference 3 which indicates that the drag coefficient of a circular cylinder at  $90^\circ$  angle of attack varies quite appreciably with Reynolds number, the drag coefficient decreasing from about 1.2 at Reynolds numbers of less than 200,000 (based on cylinder diameter) to approximately 0.3 at Reynolds numbers greater than 500,000. As previously indicated, the range of Reynolds numbers (80,000 to 255,000) tested on the fuselage alone is partly within this critical range where the drag changes abruptly. These calculations in reference 2 indicate that this variation in drag or normal-force coefficient ( $C_D = C_Z$  at  $90^\circ \alpha$ ) with Reynolds numbers has a corresponding large effect on the pitching-moment coefficients.

A comparison was made between the results obtained from tests of the fuselage alone and results calculated by a method given in reference 3. The reference presents a method for calculating the aerodynamic forces and moments on inclined bodies of revolution with blunt bases for various Reynolds numbers. For calculation purposes, the fuselage of the static model was assumed to have a blunt base ending at the jet exhaust. The portion of the fuselage rearward of this point was practically a boom and was considered small relative to the remainder of the fuselage so that its elimination for purposes of computations was assumed to have no appreciable effect on the results. The calculations were made on the premise that the fuselage was nearly a circular cylinder. The dimensional characteristics of the airplane used in calculating the forces and moments are presented on table I.

The experimental force and moment data were compared with force and moment characteristics calculated for the fuselage alone as shown in figure 15. The experimental data shown were obtained at a Reynolds number of 340,000 based on the wing mean aerodynamic chord. The corresponding calculations made in accordance with reference 3 were based on the fuselage maximum depth and upon the component of velocity normal to the fuselage axis, which at  $90^\circ$  angle of attack corresponds to a Reynolds number of 210,000. A variation in cross Reynolds number along the fuselage axis with variation in fuselage depth was not taken into consideration. Also, in order to obtain a calculated trend of Reynolds number effect, calculations were made at a Reynolds number equivalent to the highest value previously tested in the 7- by 10-foot tunnel which, based on the maximum depth of the fuselage of the model, is equal to 695,000 at  $90^\circ$  angle of attack. The drag coefficient of the fuselage alone at  $0^\circ$  angle of attack, required in the computations, was obtained from measurements on the model (fig. 14). The calculated values of  $C_m$ ,  $C_L$ , and  $C_D$  for the fuselage alone were in fairly good agreement with corresponding experimental values at low angles of attack. The calculated values of  $C_m$  and  $C_D$  at high angles of attack, however, did not agree with the experimental data although the calculated lift data were in fair agreement. The discrepancy between the calculated and experimental data may be in part accounted for by the deviation of the fuselage tested from a body of revolution. A comparison of the calculated pitching-moment coefficients at Reynolds numbers of 210,000 and 695,000 indicates a large decrease in the unstable pitching moment of the fuselage with the increase in Reynolds number. Correspondingly, the value of  $C_D$  decreased. These trends are consistent with those obtained experimentally on the fuselage alone for a smaller range of Reynolds numbers.

Wing alone.— The variations of  $C_m$  and  $C_z$  with angles of attack for various Reynolds numbers for the wing-alone condition are plotted in figure 16. The wing alone had a nose-down  $C_m$  for all angles of attack and Reynolds numbers. The values of  $dC_m/d\alpha$  indicated, in general, that

~~CONFIDENTIAL~~  
SECURITY INFORMATION

NACA RM L50L19

15

the wing was stable for all angles of attack. There appeared to be little change in  $C_m$  due to variations in Reynolds number. From an angle of attack of  $15^\circ$  to  $60^\circ$ , there was a slight tendency for  $C_z$  to increase with increasing Reynolds number (fig. 16).

Fuselage plus wing.- Figure 17 presents the variation of  $C_m$  and  $C_z$  with angle of attack for various Reynolds numbers for the fuselage-plus-wing combination. There generally was no appreciable effect of Reynolds number on  $C_m$  below the stall ( $\alpha = 14^\circ$ ) although beyond the stall the unstable  $C_m$  of the fuselage-plus-wing combination decreased as the Reynolds number increased. There did not appear to be an appreciable effect of Reynolds number on  $C_z$  of the combination up to approximately  $50^\circ$  angle of attack. Beyond this angle of attack there was no consistent Reynolds number effect.

Fuselage plus horizontal tail.- The variation of  $C_m$  and  $C_z$  with angle of attack for various Reynolds numbers for the fuselage-plus-horizontal-tail combination is presented in figure 18. The addition of the horizontal tail to the fuselage made it stable in pitch up to  $14^\circ$  angle of attack where it appeared that the horizontal tail stalled; the magnitude of the nose-up  $C_m$  at any angle of attack for the fuselage plus tail was less than that of the fuselage alone. The variation of  $C_z$  with angle of attack was also similar to that for the fuselage alone although the magnitude of  $C_z$  at any angle of attack was greater for the fuselage-plus-tail combination. Reynolds number effects on  $C_m$  and  $C_z$  were similar to those obtained for the fuselage alone.

#### Comparison of Reynolds Number Effects on Results of

##### Component Parts and Complete Model

Comparison of the results obtained on component parts of the model with those obtained on the complete model for a Reynolds number range from 130,000 to 413,000 indicated that the pitching-moment change obtained was primarily a result of a change in the pitching moment of the fuselage alone. As previously indicated, increasing the Reynolds number led to a decrease in the normal-force coefficient for the fuselage alone; there was, however, no change in the normal-force coefficient for the complete model. Inasmuch as results obtained for the wing alone indicated no appreciable change in normal-force coefficient, it appears that compensating changes in normal-force coefficient due to Reynolds number may be contained in interference effects between various parts of the model and in possible small unmeasurable effects on the wing and horizontal tail.

~~CONFIDENTIAL~~  
SECURITY INFORMATION



### Mach Number Effects

The force and moment data discussed thus far in the paper are applicable only at very low Mach numbers. The effects of compressibility, as indicated in reference 3, would be such as to increase the drag of a circular cylinder at  $90^\circ$  angle of attack to approximately the same order of magnitude as obtained at very low Reynolds numbers. Inasmuch as the instability of the complete model of this design at low Reynolds number was believed attributable mainly to the associated high drag of the fuselage at high angles of attack, calculations were made as suggested in reference 2 to determine the pitching moment of the model fuselage at a high Mach number, again on the premise that it was nearly a circular cylinder. The calculations were made by the method of reference 3, based upon the component of velocity normal to the fuselage axis, and were arbitrarily made for a Mach number of 0.9 at standard sea-level conditions. At  $90^\circ$  angle of attack, the corresponding Reynolds number was 3,440,000. The equations for lift, drag, and pitching moment in reference 3 include terms which are influenced by both viscous and potential effects. Consideration of viscous effects at high-subsonic Mach numbers was made in accordance with reference 3. The potential effects were corrected approximately for high-subsonic Mach numbers by the Prandtl-Glauert relation. The calculated values of the lift, drag, and pitching-moment coefficients for this high-subsonic Mach number have been plotted in figure 15 and show that beyond approximately  $30^\circ$  angle of attack the values are actually somewhat greater in magnitude than those obtained previously at lower Reynolds and Mach numbers. The pitching-moment results indicate unsatisfactory stability characteristics for the fuselage alone similar to those indicated for the very low Reynolds numbers. Based on unpublished data from the Langley 24-inch high-speed tunnel, it appears the compressibility effects on the wing and tail surfaces will provide only a small increase in the stability of the airplane at high angles of attack. Thus, based on apparent large compressibility effects on the fuselage, it appears that the airplane may trim at high angles of attack at high Mach numbers.

### Asymmetry in Rolling and Yawing Moments

Although the data are not presented, it is interesting to note that results from tests of the static model at  $0^\circ$  yaw both in the spin tunnel and the 7- by 10-foot tunnel showed asymmetric rolling and yawing moments acting on the model above approximately  $16^\circ$  angle of attack. The direction of both moments changed occasionally as the angle of attack increased. The magnitude of the rolling and yawing moments increased to a maximum at approximately  $60^\circ$  angle of attack where the fuselage is completely stalled. As the Reynolds number was increased, the magnitude of the moments decreased and it thus appears that the phenomenon could be associated only with low Reynolds numbers.

C O N C L U S I O N S

On the basis of tests in the Langley 20-foot free-spinning tunnel of a dynamic model representative of a supersonic airplane having an extremely long nose and small wing and on the basis of force tests of a static model in both the spin tunnel and in the Langley 300 MPH 7- by 10-foot tunnel through a Reynolds number range from approximately 130,000 to 1,124,000 the following conclusions are made:

1. Although there appeared to be no appreciable effects of Reynolds number on the pitching-moment coefficients of the complete model at low angles of attack, a large scale effect was indicated on the pitching-moment coefficients at high angles of attack. At very high angles of attack, trim conditions were obtained for low Reynolds numbers, whereas at higher Reynolds numbers the trim conditions disappeared.

2. Based on the static pitching-moment characteristics alone, the results indicated that a corresponding airplane at low-subsonic Mach numbers probably would not have a high-angle-of-attack trim condition; however, calculations indicated that at high-subsonic Mach numbers it might be possible for the airplane to trim at high angles of attack.

3. There appeared to be no appreciable scale effect on the force coefficients for the complete model from  $0^\circ$  to  $90^\circ$  angle of attack.

4. The results of the investigation, in general, indicate that scale effect may appreciably influence free dynamic results obtained at low Reynolds numbers and high angles of attack on a design having a very long nose and a very small wing.

Langley Aeronautical Laboratory  
National Advisory Committee for Aeronautics  
Langley Field, Va.

REFERENCES

1. Stone, Ralph W., Jr., Burk, Sanger M., Jr., and Bihrlle, William, Jr.:  
The Aerodynamic Forces and Moments on a  $\frac{1}{10}$ -Scale Model of a  
Fighter Airplane in Spinning Attitudes as Measured on a Rotary  
Balance in the Langley 20-Foot Free-Spinning Tunnel. NACA TN 2181,  
1950.
2. Bauer, C., and Kleckner, H.: Notes on the Behavior of the X-3 Airplane  
at Extreme Angles of Attack. Rep. No. SM-13716, Douglas Aircraft Co.,  
Inc., Feb. 22, 1950.
3. Allen, H. Julian: Estimation of the Forces and Moments Acting on  
Inclined Bodies of Revolution of High Fineness Ratio. NACA RM A9I26,  
1949.

TABLE I

## DIMENSIONAL CHARACTERISTICS OF THE X-3 AIRPLANE

Over-all length, ft . . . . .	62.7
Wing:	
Span, ft . . . . .	22.7
Area, sq ft . . . . .	166.5
Airfoil section . . . . .	Modified hexagon
Thickness ratio, percent chord . . . . .	4.5
Aspect ratio . . . . .	3.1
Taper ratio . . . . .	0.388
Incidence, deg . . . . .	0
Dihedral, deg . . . . .	0
Sweepback (50-percent-chord line), deg . . . . .	8
Mean aerodynamic chord, ft . . . . .	7.84
Leading edge of mean aerodynamic chord rearward of leading edge root chord, ft . . . . .	2.06
Ailerons:	
Area rearward of hinge line . . . . .	8.5
Span, percent wing span . . . . .	29.8
Flaps:	
Leading-edge flap:	
Area (forward of hinge line), sq ft . . . . .	17.3
Span, percent wing span . . . . .	73.2
Trailing-edge flap:	
Area (rearward of hinge line), sq ft . . . . .	18.5
Span, percent wing span . . . . .	44.6
Horizontal tail surface:	
Total area, sq ft . . . . .	31.0
Span, ft . . . . .	9.8
Airfoil section . . . . .	Modified hexagon
Thickness ratio, percent chord . . . . .	4.5
Aspect ratio . . . . .	3.0
Taper ratio . . . . .	0.400
Dihedral, deg . . . . .	0
Sweepback (50-percent-chord line), deg . . . . .	23
Distance from center of gravity to hinge line of horizontal tail surface, ft . . . . .	21.4



TABLE I

## DIMENSIONAL CHARACTERISTICS OF THE X-3 AIRPLANE - Concluded

## Vertical tail surface:

Total area, sq ft	23.7
Rudder area rearward of hinge line	6.1
Airfoil section	Modified hexagon
Thickness ratio, percent chord	4.5
Aspect ratio	1.3
Taper ratio	0.298
Sweepback (50-percent-chord line), deg	30

## Dimensional characteristics used in calculating force and moment characteristics of fuselage alone:

Base area (cross-sectional area at jet exit), sq ft	13.7
Plan-form area of fuselage (nose to jet exit), sq ft	211.0
Fuselage length (nose to jet exit), ft	50.5
Distance to moment center from nose, ft	37.3
Distance to centroid of plan-form area from nose, ft	32.1
Reference area for coefficient evaluation (wing area), sq ft	166.5
Reference length for coefficient evaluation (M.A.C. of wing), ft	7.84
Fineness ratio (nose to jet exit)	8.27



TABLE II

## MASS CHARACTERISTICS AND INERTIA PARAMETERS FOR LOADING CONDITIONS

TESTED ON DYNAMIC MODEL

[Model values converted to corresponding full-scale values;  
moments of inertia are given about center of gravity]

Loading	Weight (lb)	Airplane relative density, $\mu$		Moments of inertia (slug-ft <sup>2</sup> )			Inertia parameters		
		Sea level	Test altitude (40,000 ft)	$I_X$	$I_Y$	$I_Z$	$\frac{I_X - I_Y}{mb^2}$	$\frac{I_Y - I_Z}{mb^2}$	$\frac{I_Z - I_X}{mb^2}$
Minimum flying weight	15,031	52.00	212.3	4,274	49,083	49,345	$-1864 \times 10^{-4}$	$-11 \times 10^{-4}$	$1875 \times 10^{-4}$
Design gross weight	20,828	72.04	294.10	5,381	63,071	65,559	$-1732 \times 10^{-4}$	$-75 \times 10^{-4}$	$1807 \times 10^{-4}$

NACA

TABLE III

## GLIDE TESTS OF DYNAMIC MODEL

[Ailerons and rudder neutral; model released into air stream moving approximately 50 ft/sec]

Horizontal tail setting (deg)	Initial angle of attack (deg)	Behavior of model
10	90	Pitched down to $\alpha = 70^\circ$
10	80	Do.
10	70	Remained at $\alpha = 70^\circ$
10	60	Pitched up to $\alpha = 70^\circ$
10	55	Do.
10	50	Do.
10	45	Do.
10	40	Do.
10	35	Do.
10	30	Do.
10	27	Do.
10	26	Pitched either up or down
10	25	Pitched down and inverted
10	20	Do.
10	15	Do.
0	20	Pitched up to $\alpha = 70^\circ$
0	19	Do.
0	17	Pitched down to $\alpha = 0^\circ$
0	15	Do.
0	13	Do.
0	10	Do.
0	0	Remains at $\alpha = 0^\circ$
$-2\frac{1}{2}$	0	Pitched up to $\alpha = 70^\circ$
$-2\frac{1}{2}$	-10	Do.
$-2\frac{1}{2}$	-15	Do.
-5	0	Do.
-5	-10	Do.
-10	0	Do.
-10	-10	Do.
-25	10	Do.

TABLE IV

## TRIM-RIG TESTS OF DYNAMIC MODEL

[Ailerons and rudder neutral  
Airspeed approximately 70 feet per second]

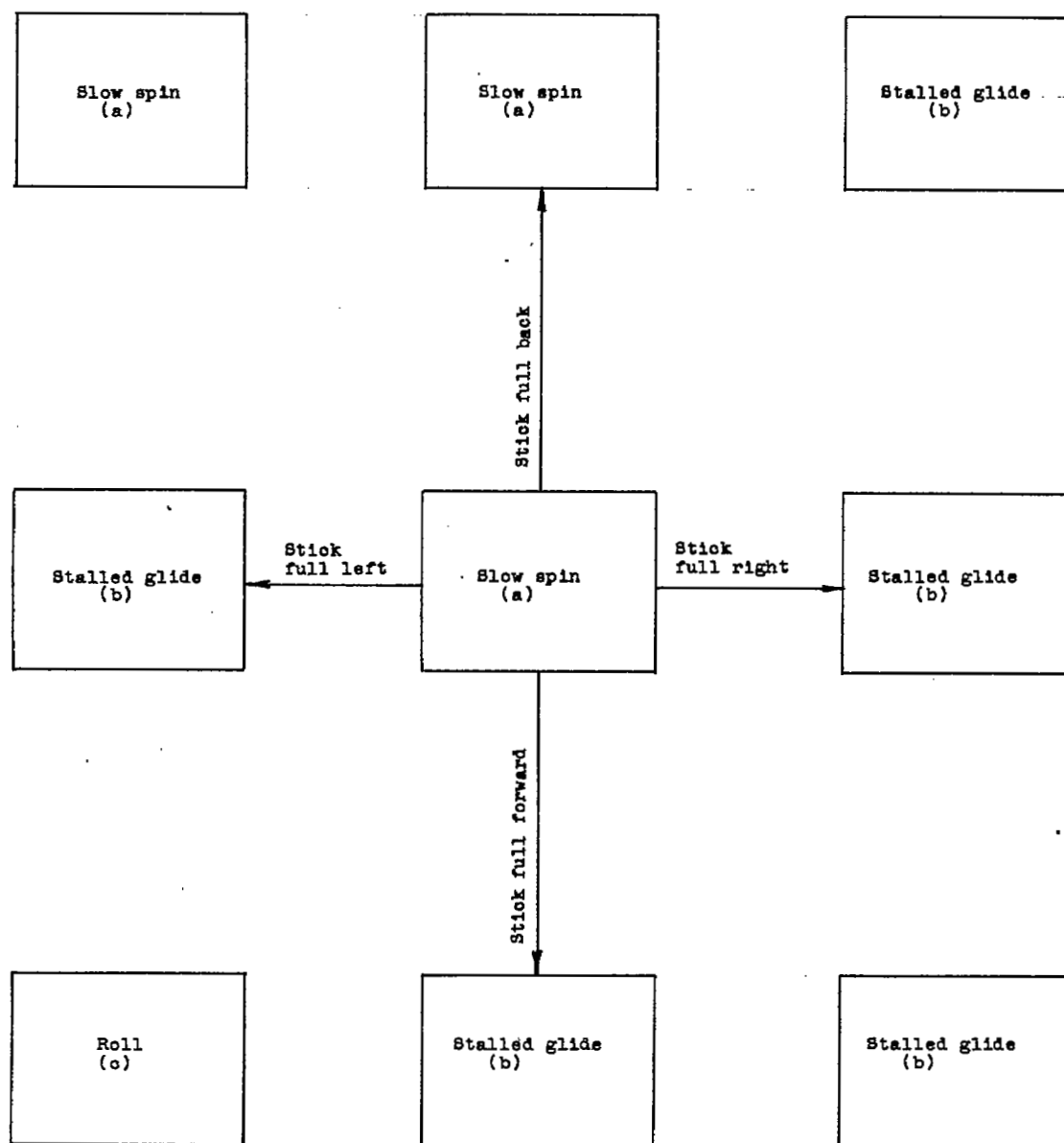
Horizontal tail settings (deg)	Trim angles (deg) (a)
0	70, 0, -60
10	70, -10, -60
-25	70, -60
-10	70, -60
-5	70, -60
$-2\frac{1}{2}$	70, (b), -60

<sup>a</sup>All angles of trim are approximate.<sup>b</sup>Almost trims at 0°.



CHART 1.- MOTIONS OF DYNAMIC MODEL IN MINIMUM FLYING WEIGHT LOADING OBTAINED DURING FREE-ROTATION TESTS

[Loading 1 on table I; landing gear and flaps retracted; model launched with rotation to the pilot's right in erect attitude; rudder deflected to right]



<sup>a</sup>Model rotates slowly at a constant rate about a vertical axis in a wide stalled gliding turn while oscillating in pitch and roll.

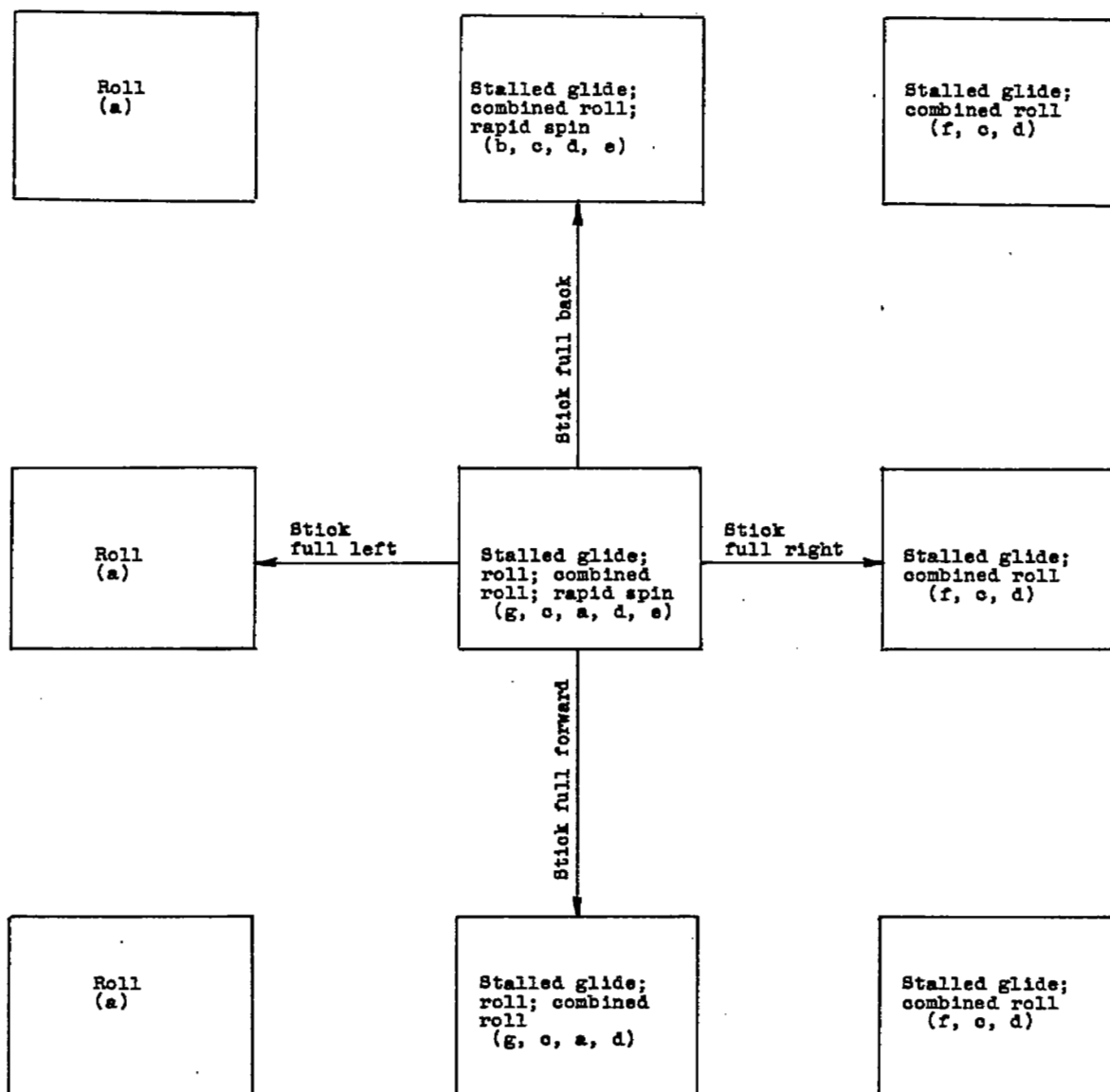
<sup>b</sup>Model glides above the stall oscillating in pitch and roll.

<sup>c</sup>Model rolls rapidly about its X-body axis while oscillating in pitch.



CHART 2.- MOTIONS OF DYNAMIC MODEL IN DESIGN GROSS WEIGHT LOADING OBTAINED DURING FREE-ROTATION TESTS

[Loading 2 on table I; landing gear and flaps retracted; model launched with rotation to the pilot's right in erect attitude; rudder deflected to right]



<sup>a</sup>Model rolls rapidly about its X-body axis while oscillating in pitch.

<sup>b</sup>Three conditions possible.

<sup>c</sup>Model glides above stall oscillating in pitch and roll.

<sup>d</sup>Model rotates moderately about a vertical axis with pitching oscillations and at the same time rolls rapidly about its X-body axis, the rotations being in the same sense.

<sup>e</sup>Model rotates at very rapid rate about its Z-body axis.

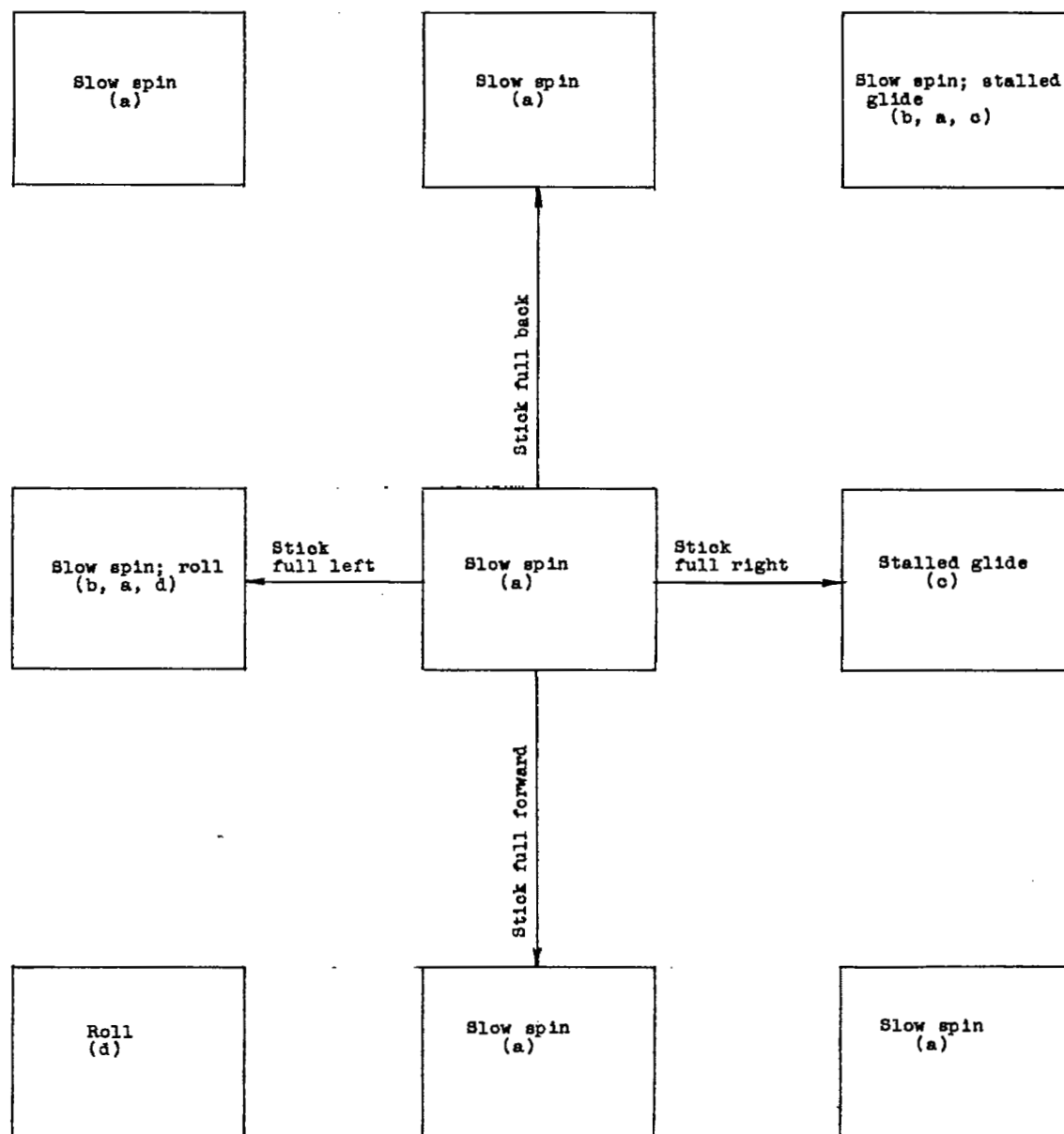
<sup>f</sup>Two conditions possible.

<sup>g</sup>Four conditions possible.



CHART 3.- MOTIONS OF DYNAMIC MODEL IN MINIMUM FLYING WEIGHT LOADING OBTAINED DURING FREE-ROTATION TESTS WITH TRAILING EDGE FLAP DEFLECTED 50°

[Loading 1 on table I; landing gear retracted; model launched with rotation to the pilot's right in erect attitude; rudder deflected to right]



<sup>a</sup>Model rotates slowly at a constant rate about a vertical axis in a wide stalled gliding turn while oscillating in pitch and roll.

<sup>b</sup>Two conditions possible.

<sup>c</sup>Model glides above stall oscillating in pitch and roll.

<sup>d</sup>Model rolls rapidly about its X-body axis while oscillating in pitch.

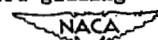
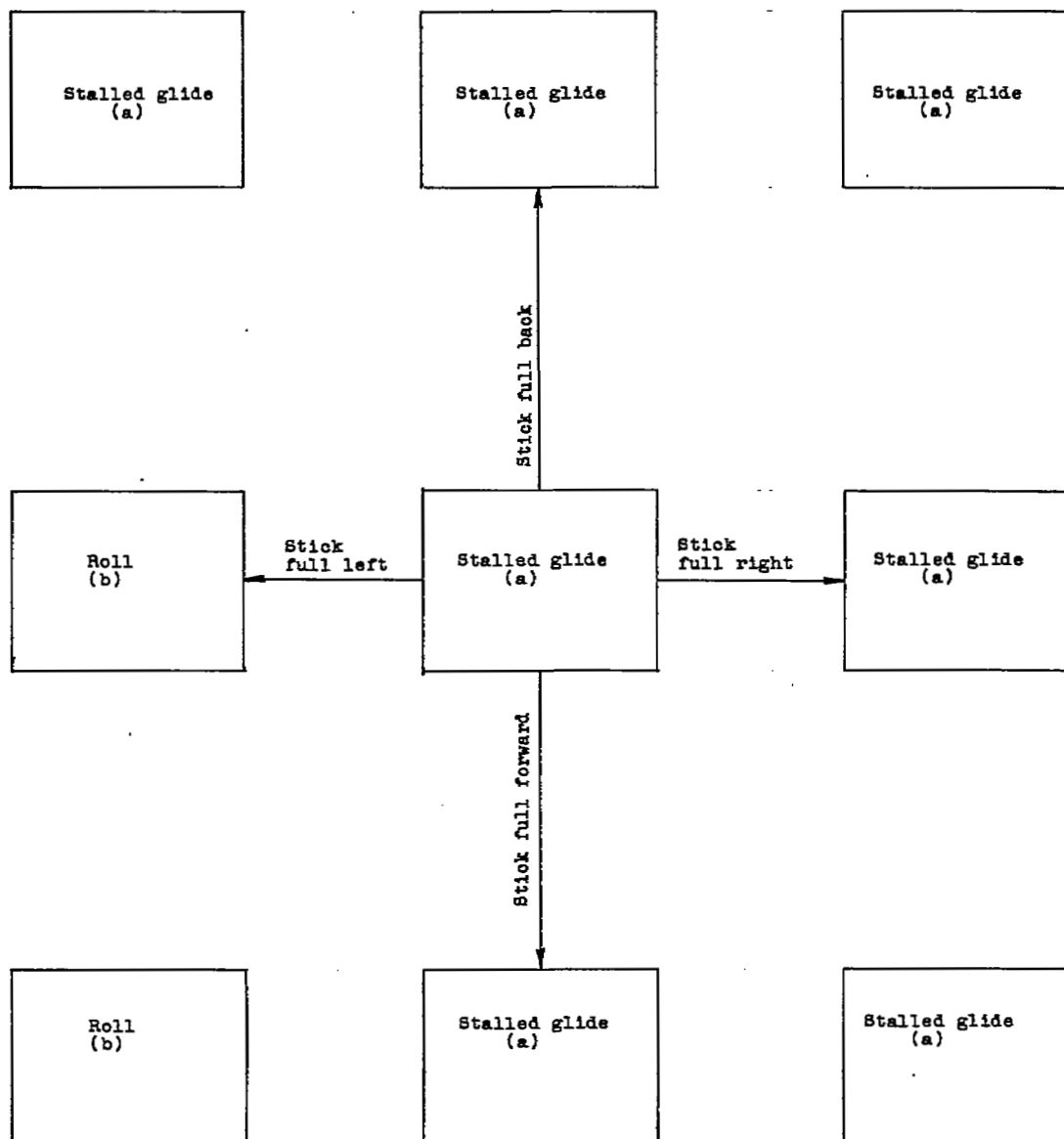


CHART 4.- MOTIONS OF DYNAMIC MODEL IN MINIMUM FLYING WEIGHT LOADING OBTAINED DURING FREE-ROTATION TESTS WITH LEADING EDGE FLAP DEFLECTED 30°

[Loading 1 on table I; landing gear retracted; model launched with rotation to the pilot's right in erect attitude; rudder deflected to right]

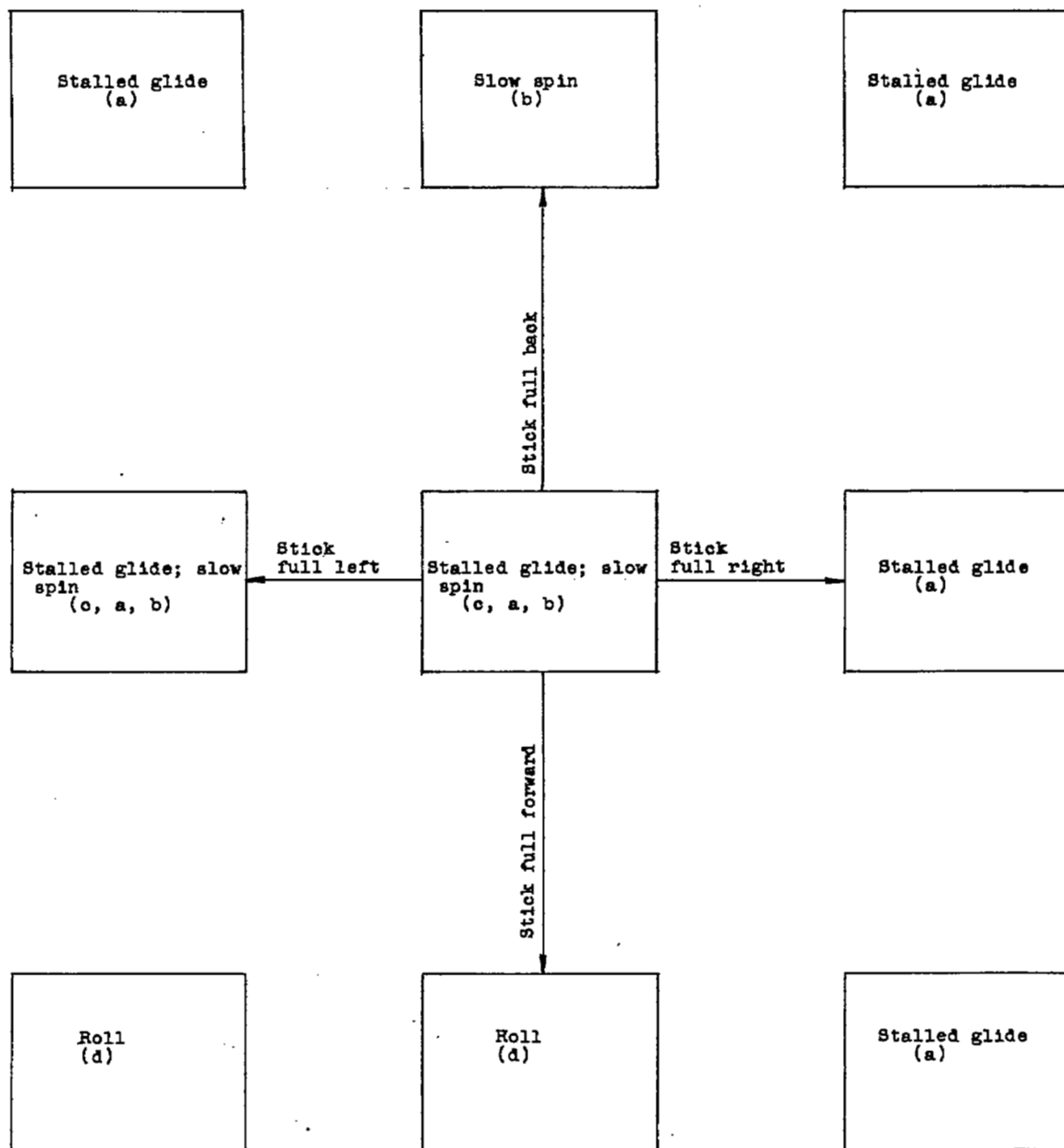


<sup>a</sup>Model glides above stall oscillating in pitch and roll.

<sup>b</sup>Model rolls rapidly about its X-body axis while oscillating in pitch.

CHART 5.- MOTIONS OF DYNAMIC MODEL IN MINIMUM FLYING WEIGHT LOADING OBTAINED DURING FREE-ROTATION TESTS WITH LEADING EDGE FLAP DEFLECTED  $30^\circ$  AND TRAILING EDGE FLAP DEFLECTED  $50^\circ$

[Loading 1 on table I; landing gear retracted; model launched with rotation to the pilot's right in erect attitude; rudder deflected to right]



<sup>a</sup>Model glides above stall oscillating in pitch and roll.

<sup>b</sup>Model rotates slowly at a constant rate about a vertical axis in a wide stalled gliding turn while oscillating in pitch and roll.

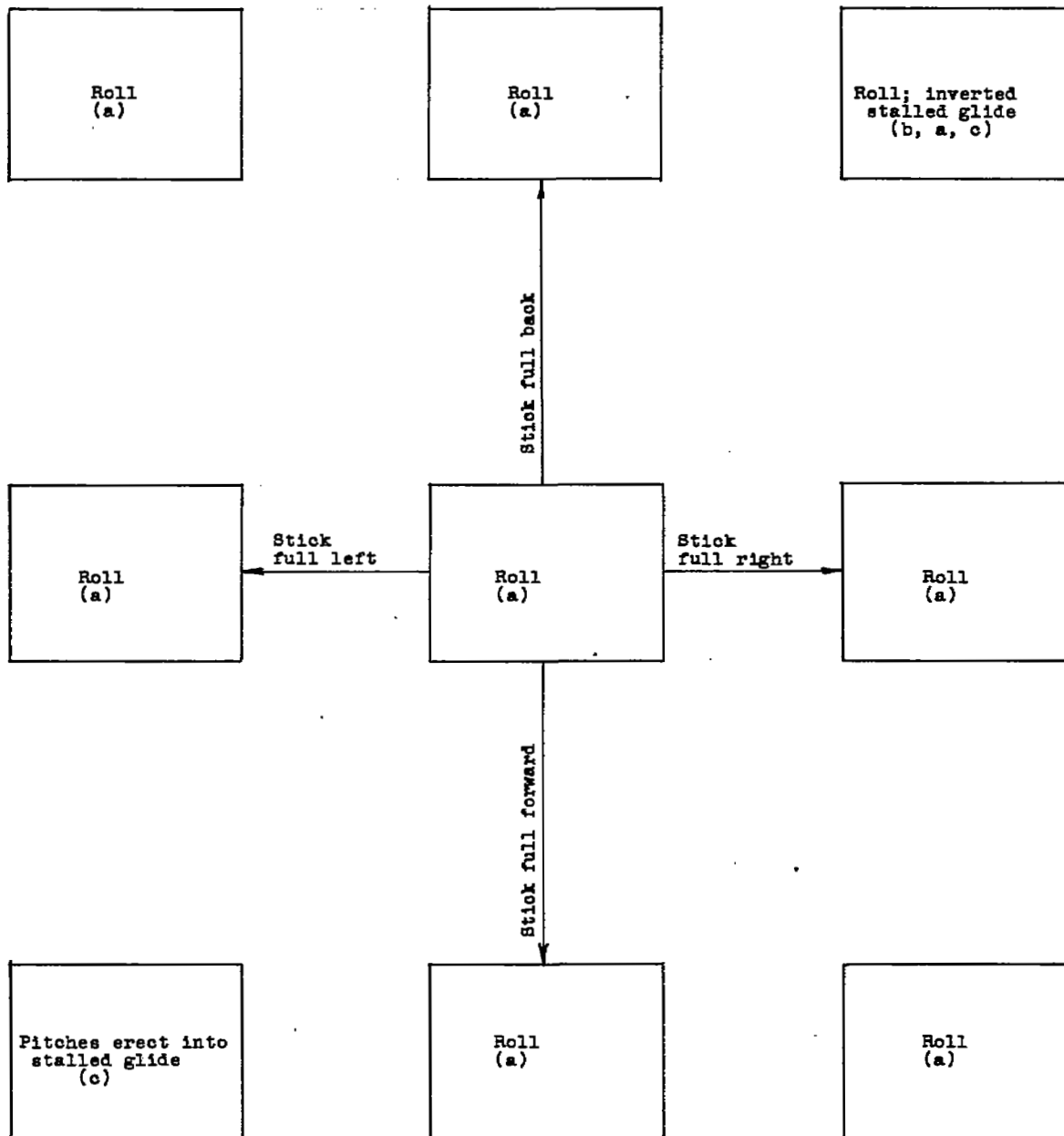
<sup>c</sup>Two conditions possible.

<sup>d</sup>Model rolls rapidly about its X-body axis while oscillating in pitch.

NACA

CHART 6.- MOTIONS OF DYNAMIC MODEL IN MINIMUM FLYING WEIGHT LOADING OBTAINED DURING FREE-ROTATION TESTS IN INVERTED ATTITUDE

[Loading 1 on table I; landing gear and flaps retracted; model launched inverted with rotation to pilot's right; rudder deflected to right]



<sup>a</sup>Model rolls rapidly about its X-body axis while oscillating in pitch.

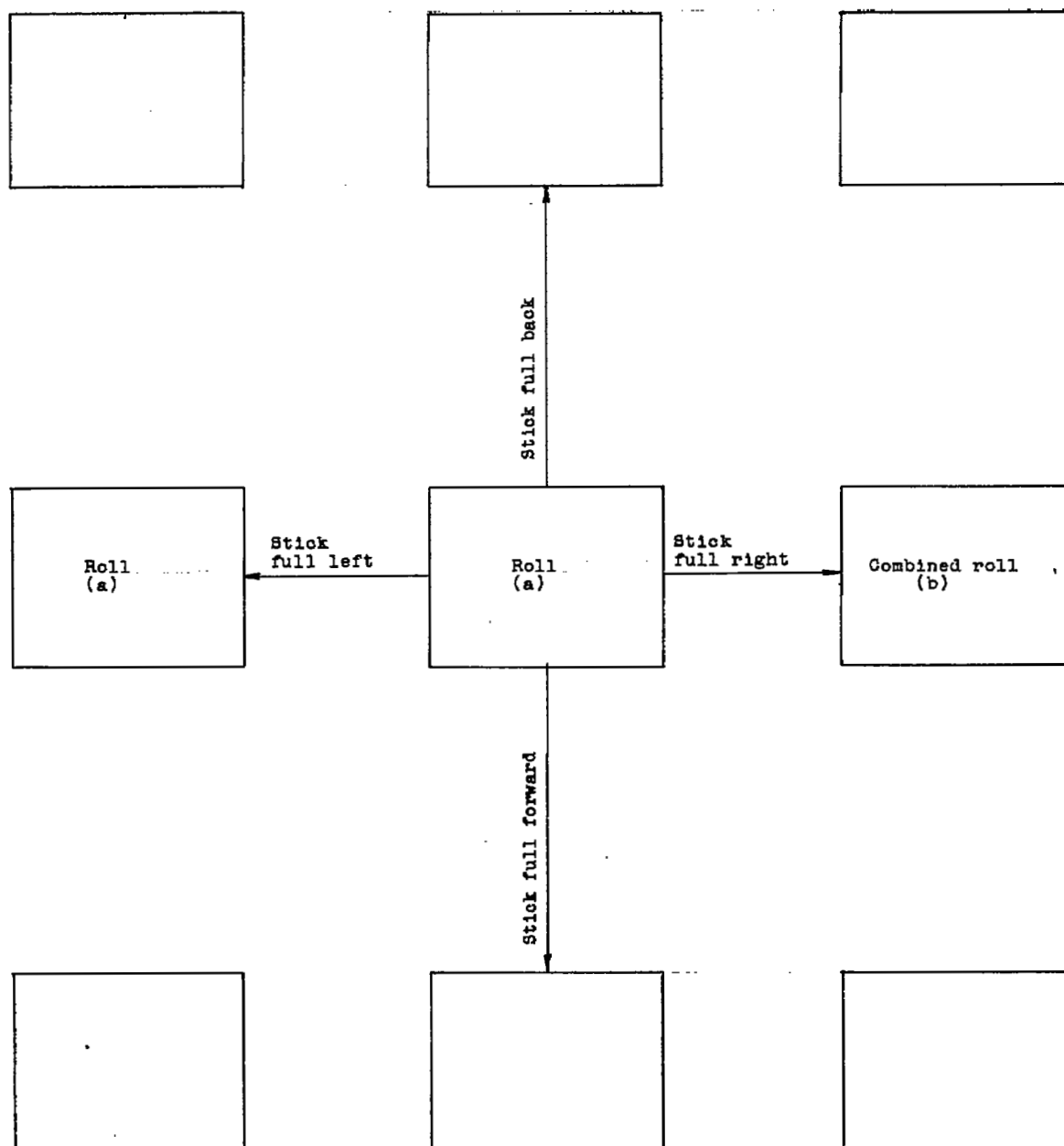
<sup>b</sup>Two conditions possible.

<sup>c</sup>Model glides above the stall oscillating in pitch and roll.



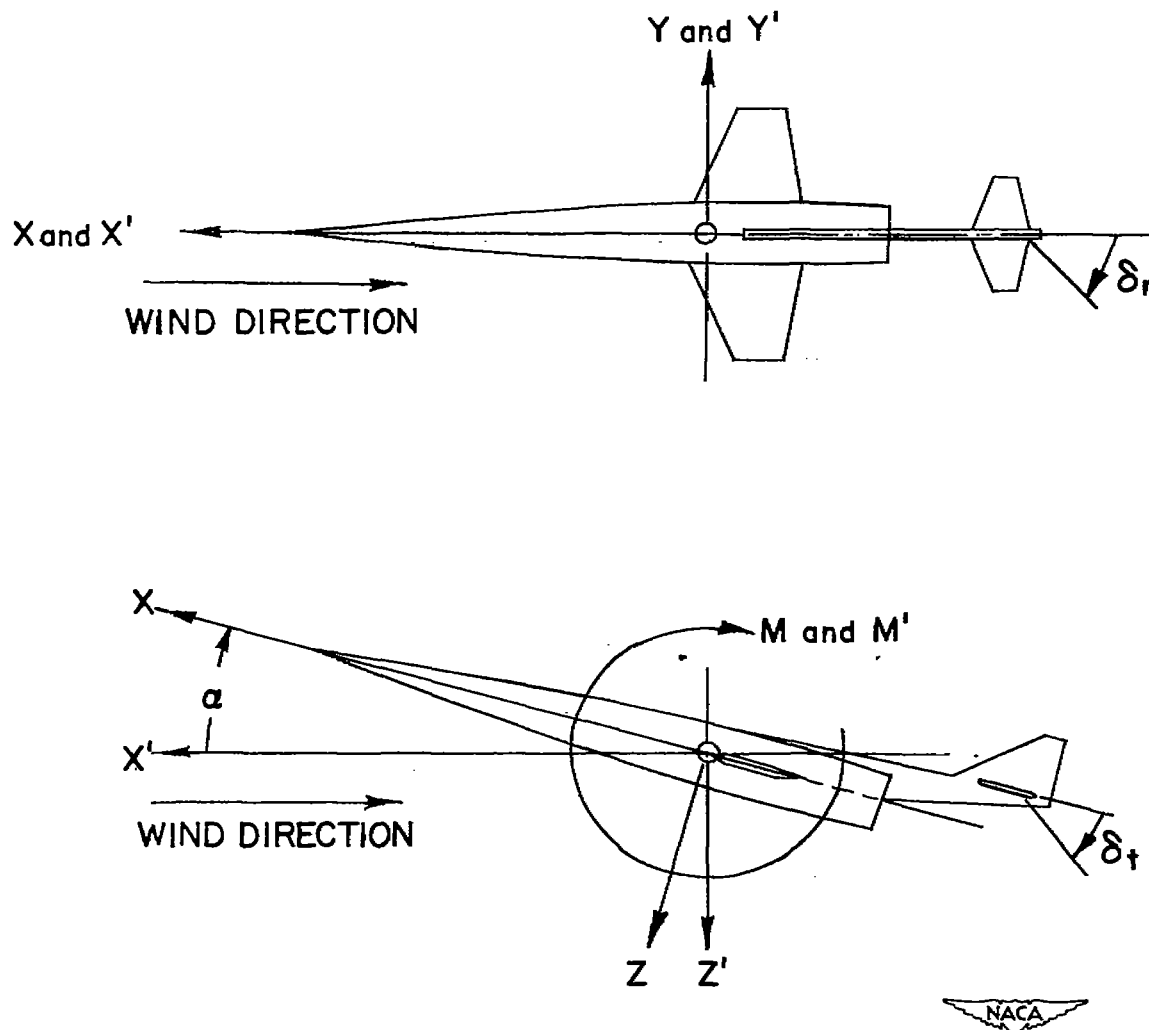
~~CONFIDENTIAL~~

[Loading 2 on table I; landing gear and flaps retracted; model launched inverted with rotation to pilot's right; rudder deflected to right]



Model rotates moderately about a vertical axis with pitching oscillations and at the same time rolls rapidly about its X-body axis, the rotations being in the same sense.

~~CONFIDENTIAL~~



PRIMED AXES ARE WIND AXES.

Figure 1.- The body and wind system of axes. Arrows indicate positive directions of forces, moments, and control-surface deflections. The body system of axes is defined as an orthogonal system having the origin at the center of gravity and in which the X-axis is the fuselage center line and the Z-axis is in the plane of symmetry and perpendicular to the X-axis and the Y-axis is perpendicular to the plane of symmetry. The wind system of axes is defined as an orthogonal system having the origin at the center of gravity and in which the Z-axis is in the plane of symmetry and perpendicular to the relative wind, the X-axis is in the plane of symmetry and perpendicular to the Z-axis, and the Y-axis is perpendicular to the plane of symmetry.



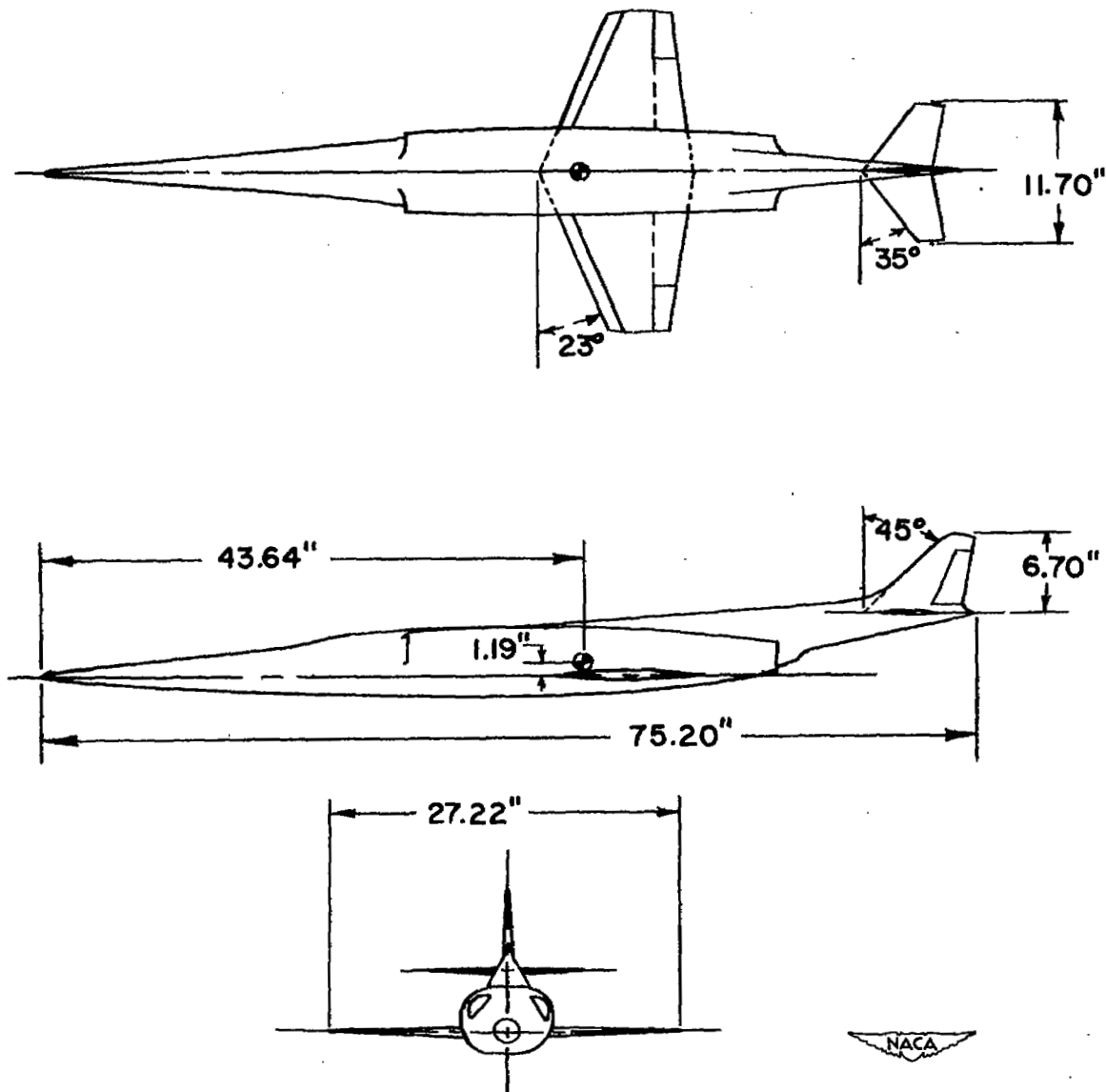


Figure 2.- Three-view drawing of static model.

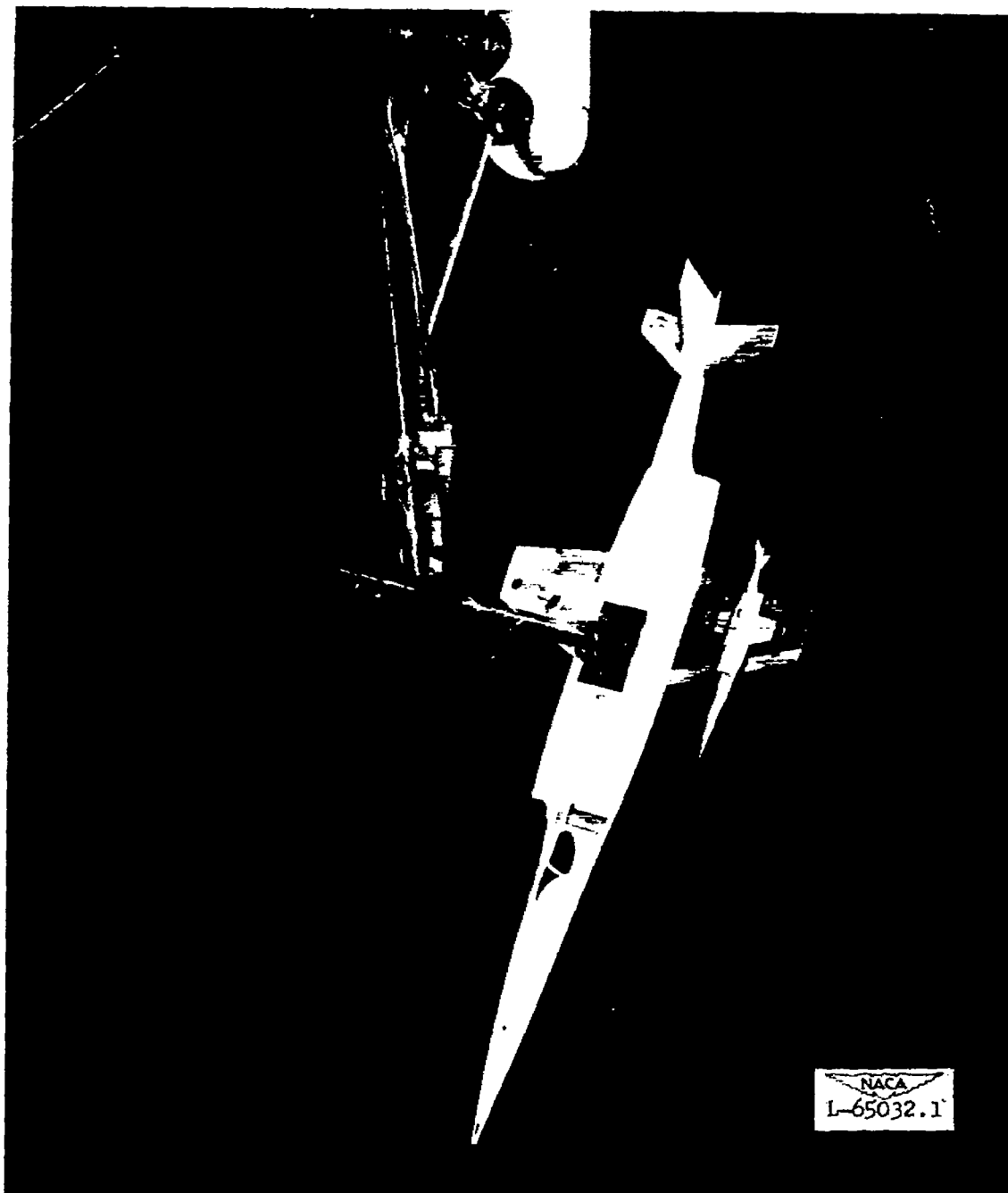
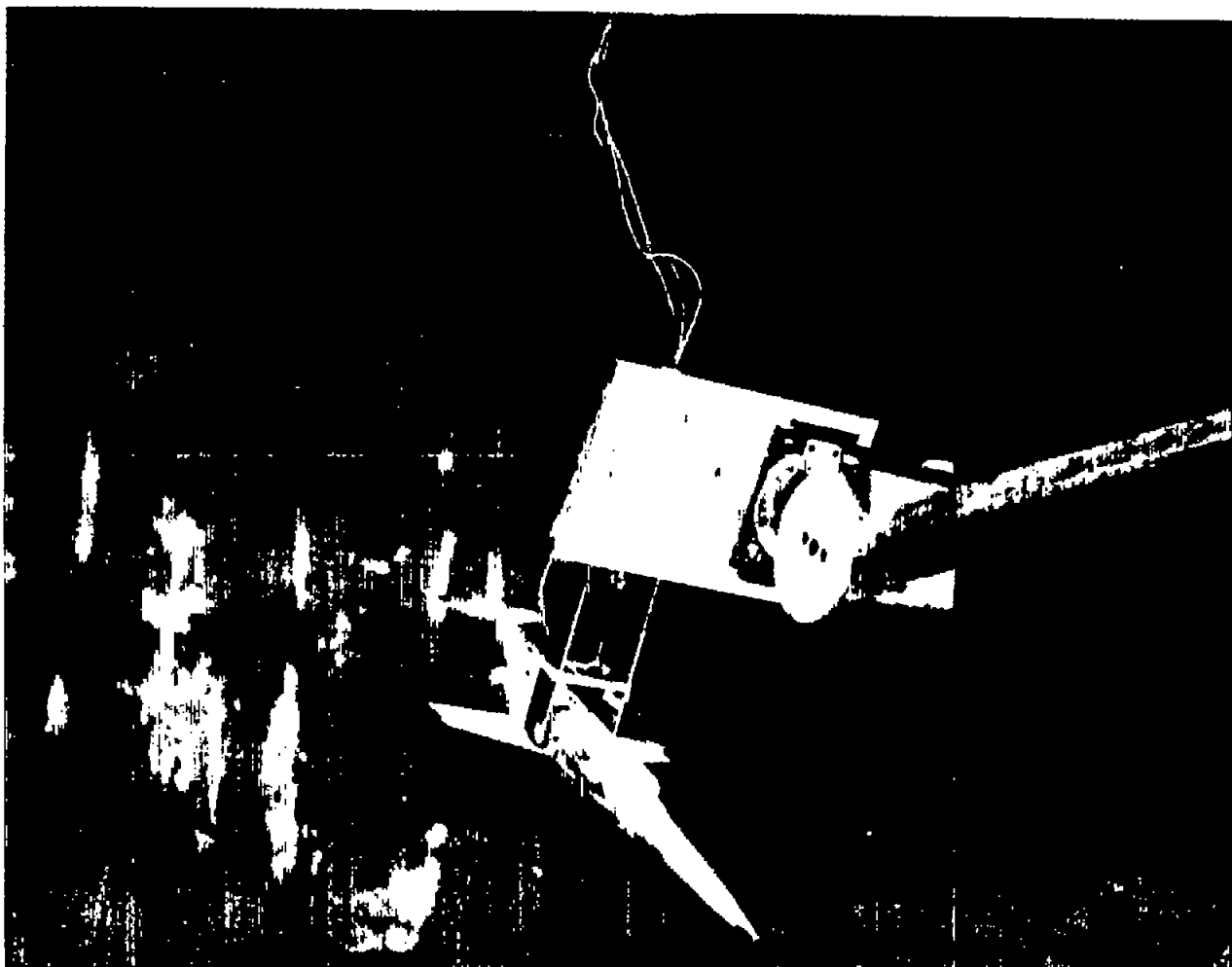


Figure 3.- Comparative sizes of the dynamic and static models ( $1/40$  and  $1/10$  scales, respectively) shown mounted in the Langley 20-foot free-spinning tunnel. Air stream is vertical.



~~CONFIDENTIAL~~  
SECURITY INFORMATION

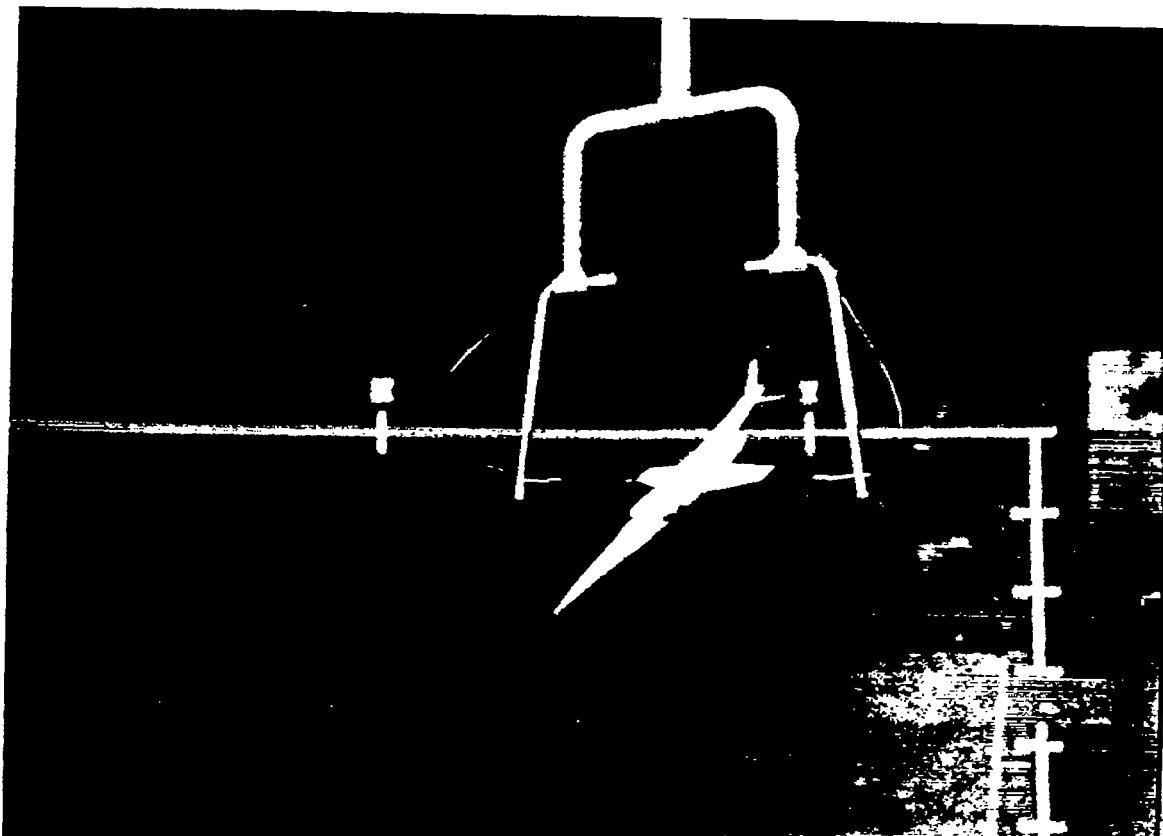


NACA  
L-66654

Figure 4.- The dynamic model clamped in rig ready to be released for glide tests into vertically rising air stream in Langley 20-foot free-spinning tunnel.

~~CONFIDENTIAL~~  
SECURITY INFORMATION





NACA  
L- 68402

Figure 5.- The dynamic model mounted on the trim rig with freedom to pitch about the Y body axis in the Langley 20-foot free-spinning tunnel.



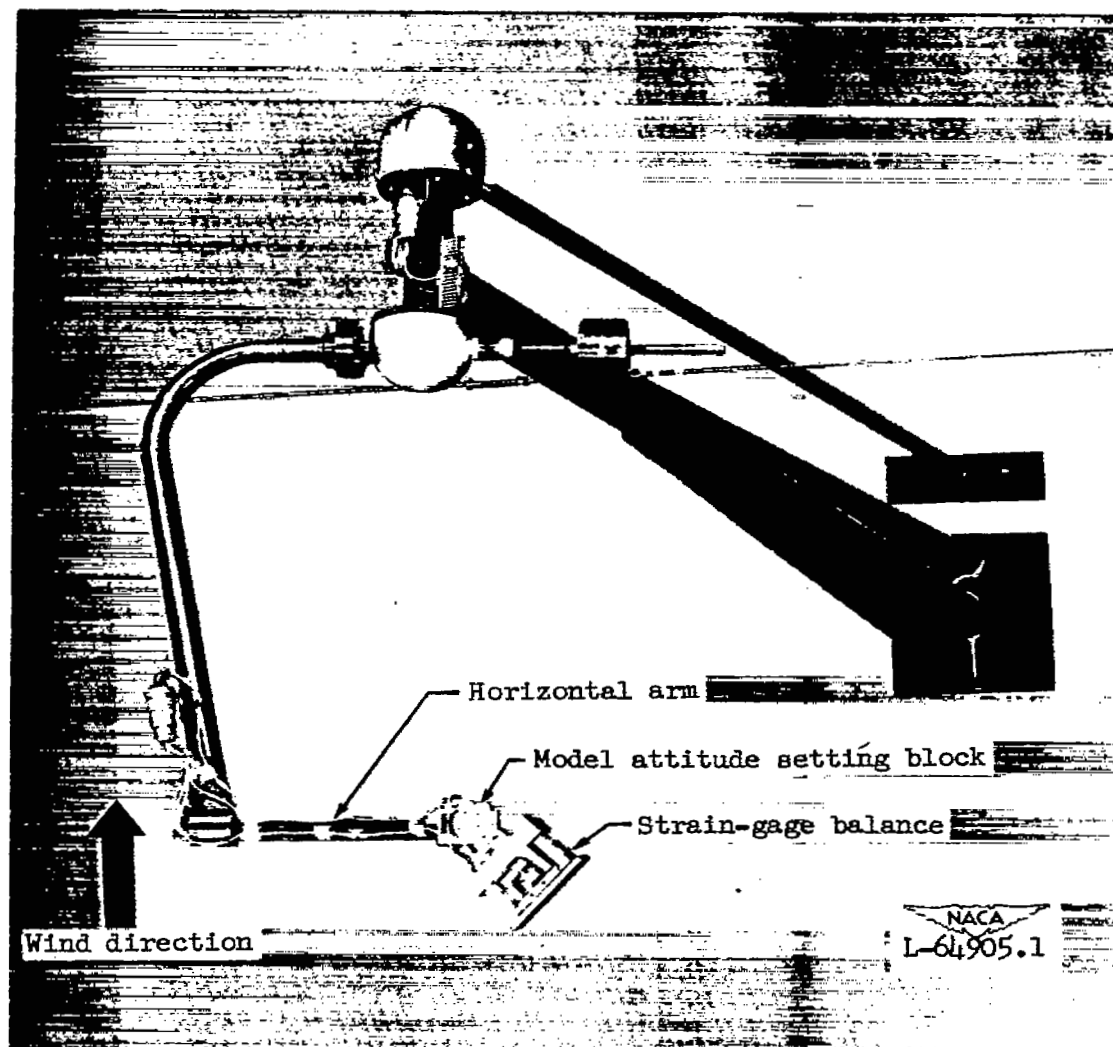
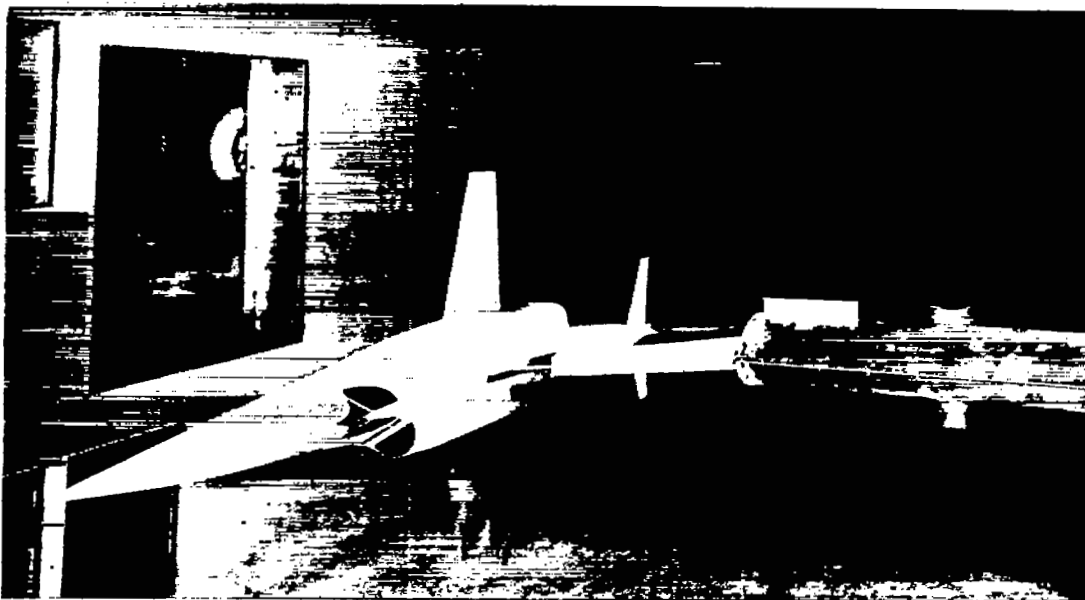


Figure 6.- The strain-gage balance in the Langley 20-foot free-spinning tunnel.

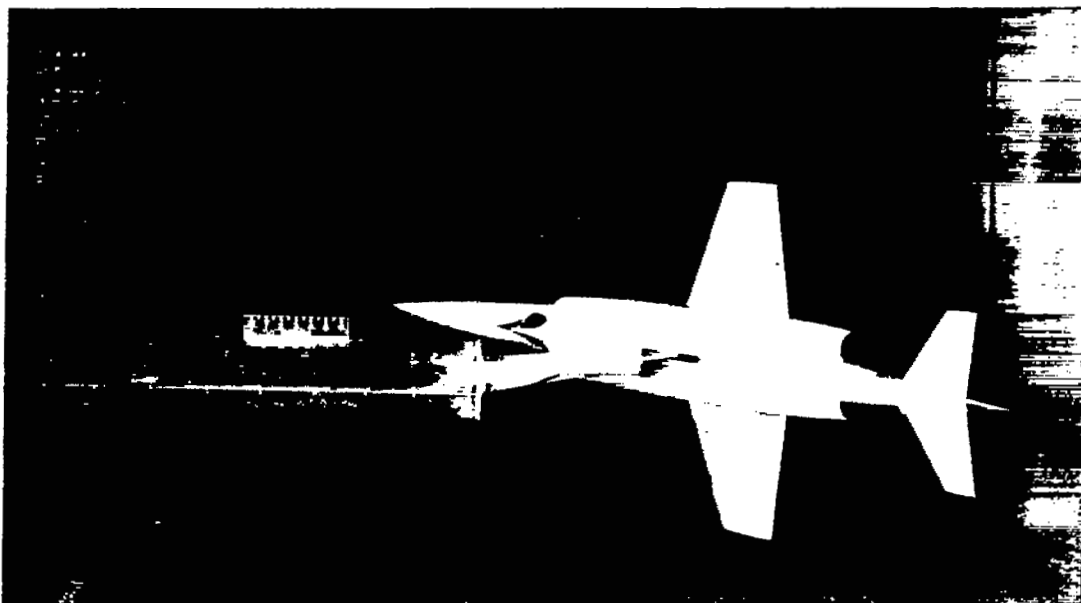






(a)  $\alpha = 0^\circ$ ; looking downstream.

NACA  
L-65584

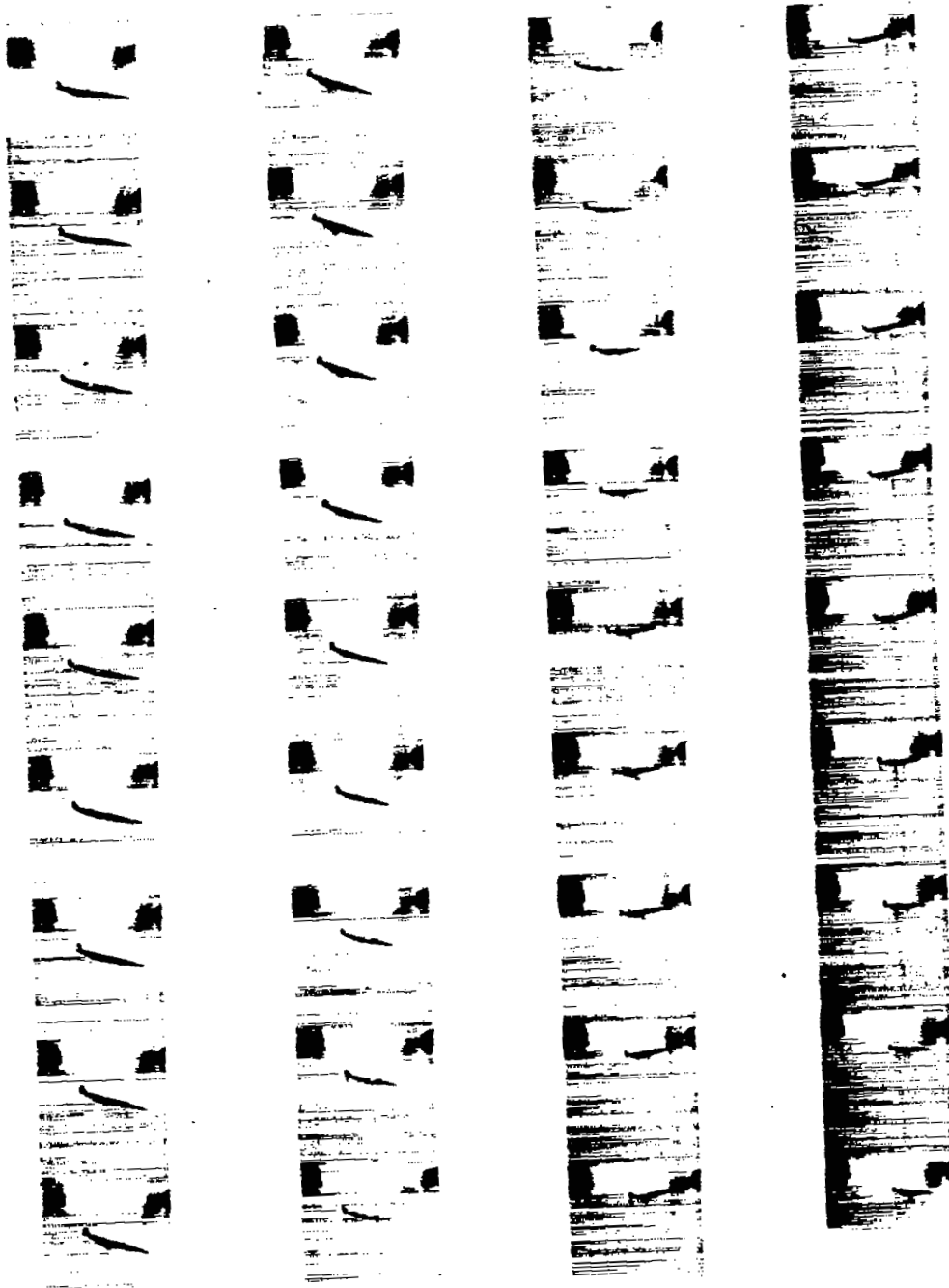


(b)  $\alpha = 60^\circ$ ; looking upstream.

NACA  
L-65586

Figure 7.- The static model mounted in the Langley 300 MPH 7- by 10-foot tunnel.



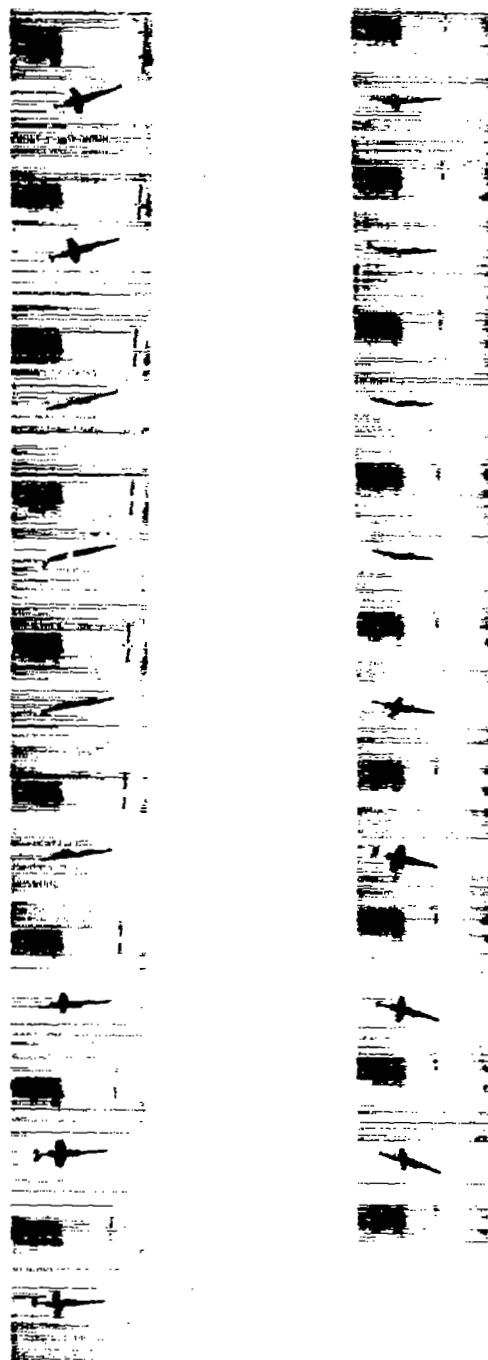


(a) Stalled gliding motion of model with oscillations in roll and pitch.

Figure 8.- Motions of the dynamic model possible after launching with spinning rotation into the spin tunnel. Camera speed, 32 frames per second.

NACA  
L-68403



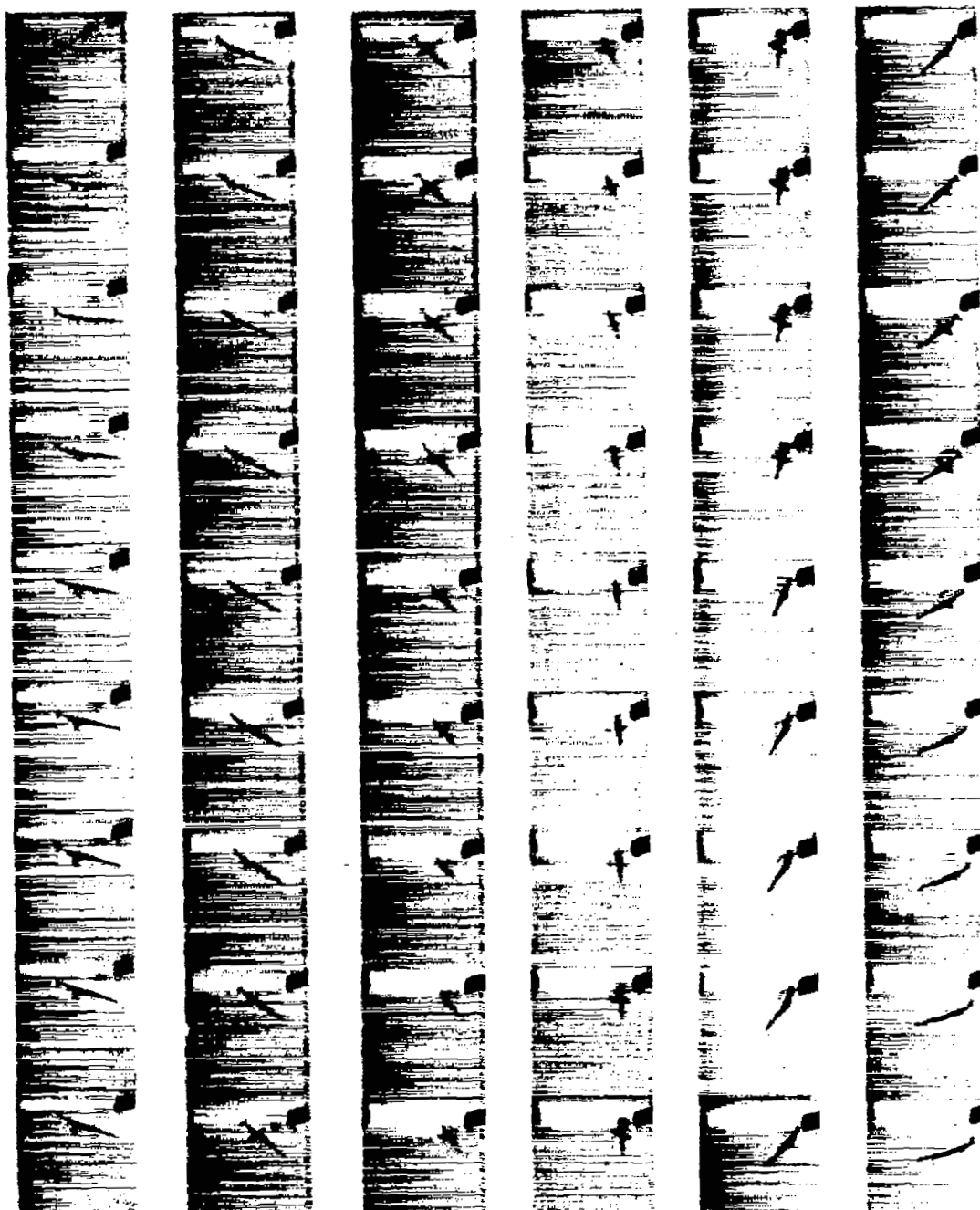


(b) Rapid rolling motion about X body axis of model with pitching oscillations.

Figure 8.- Continued.

NACA  
L-68404





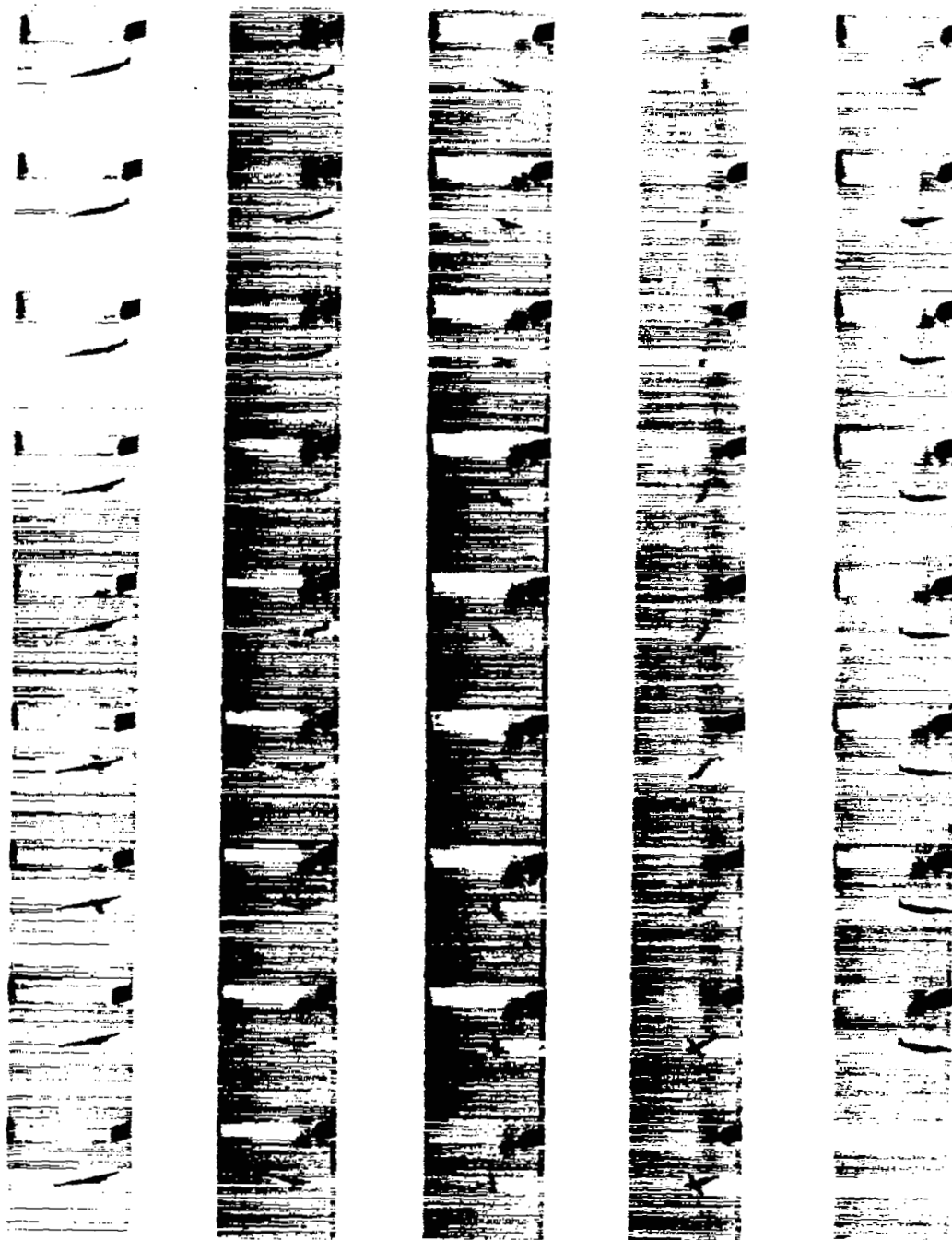
(c) Slow continued rotation of model about a vertical axis while oscillating in roll and pitch.

Figure 8.- Continued.

NACA  
L-68405






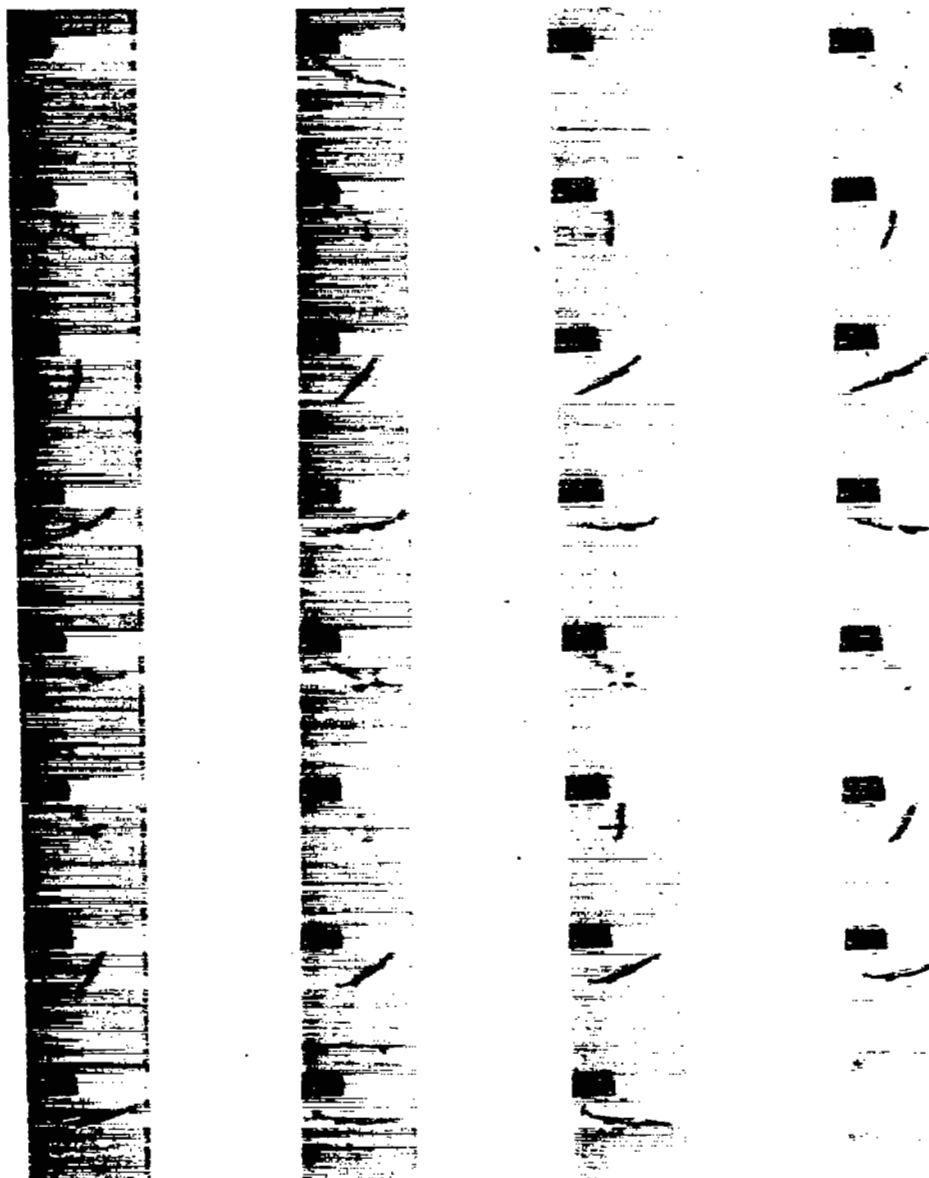


(c) Concluded.

Figure 8.- Continued.


  
L-68406



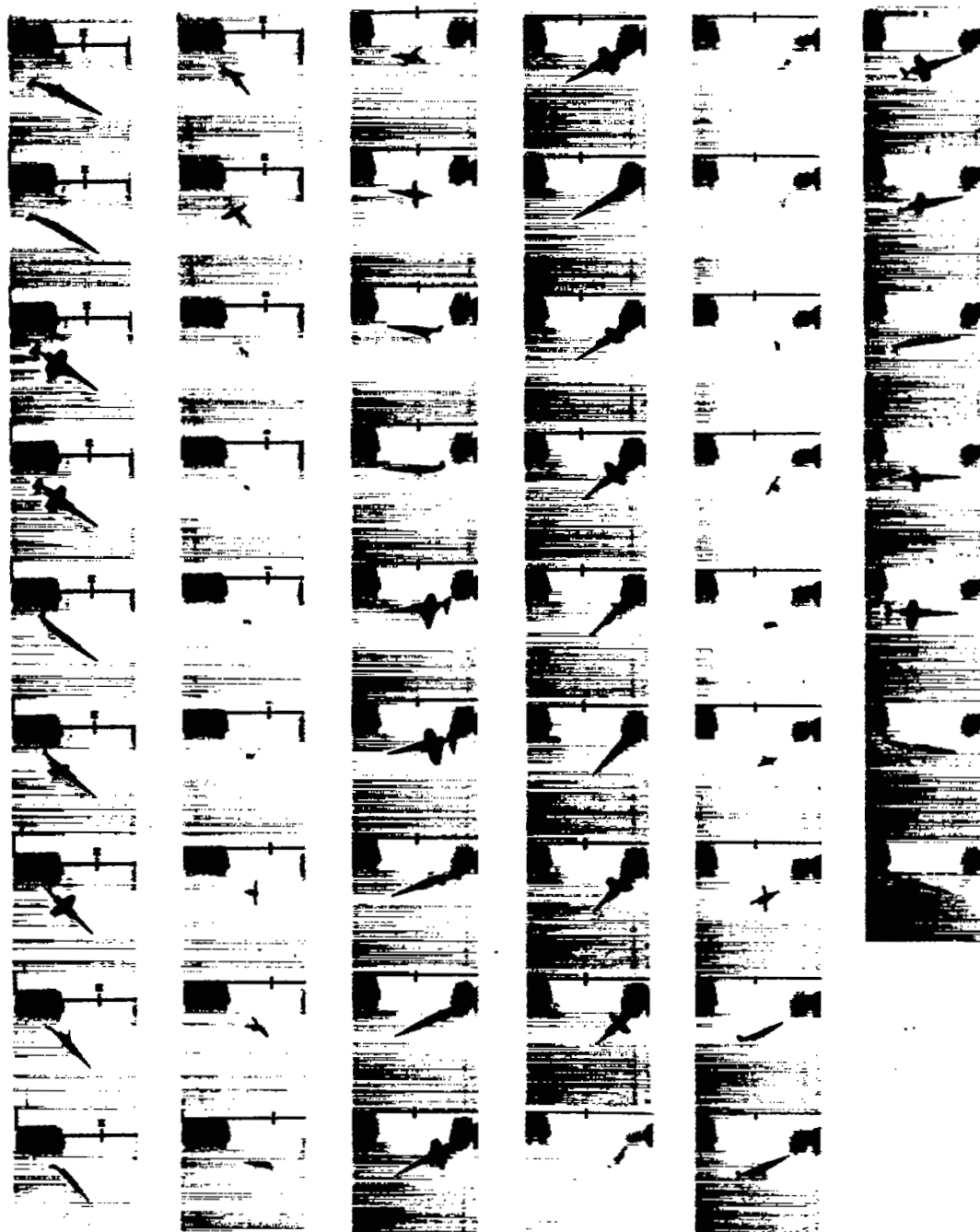


(d) Rapid rotation of model about its Z body axis while oscillating in roll and pitch.

Figure 8.- Continued.

  
L-68407

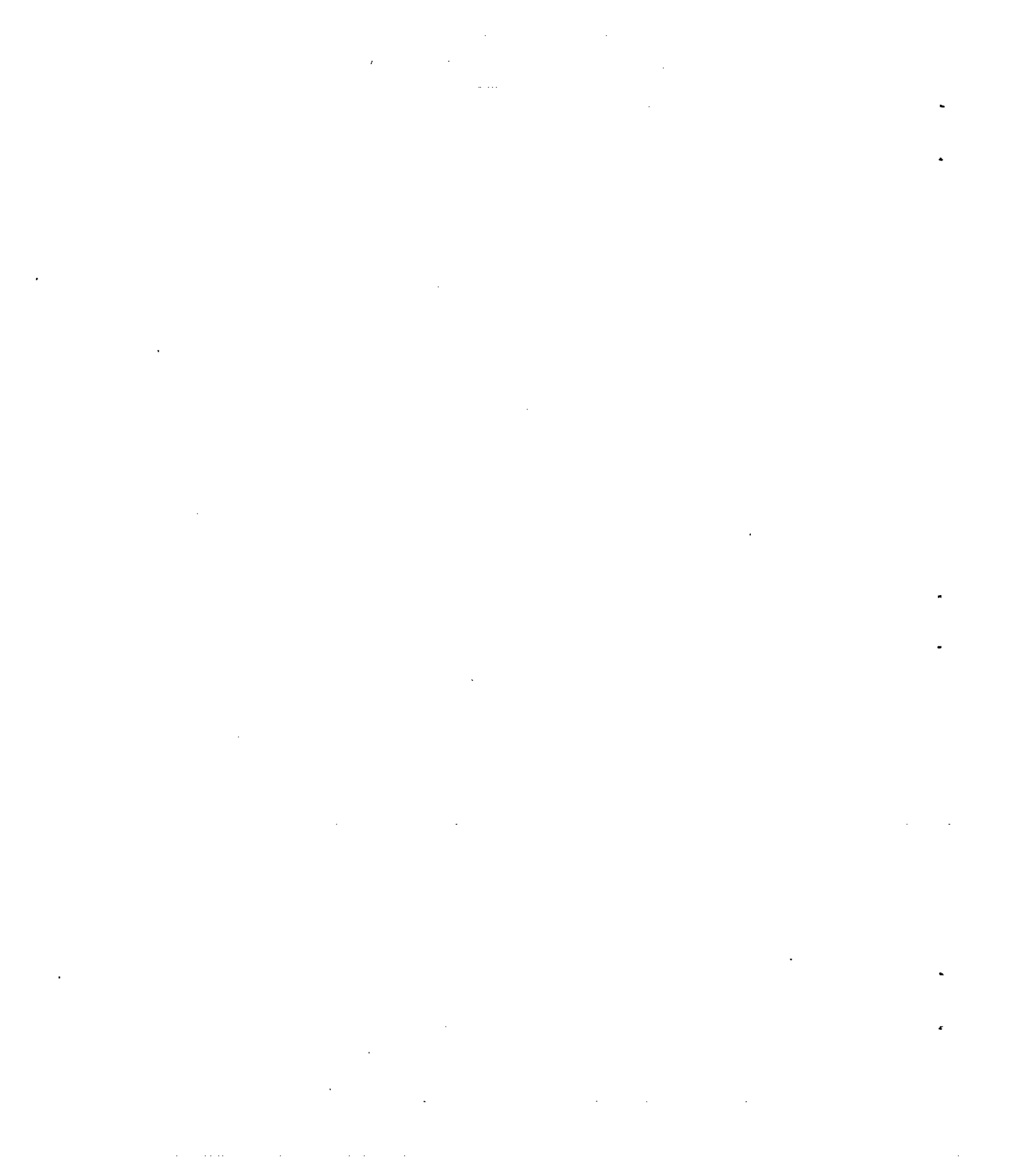




(e) Combined rotation of model about vertical axis and its X body axis while oscillating in pitch.

Figure 8.- Concluded.

NACA  
L-68408



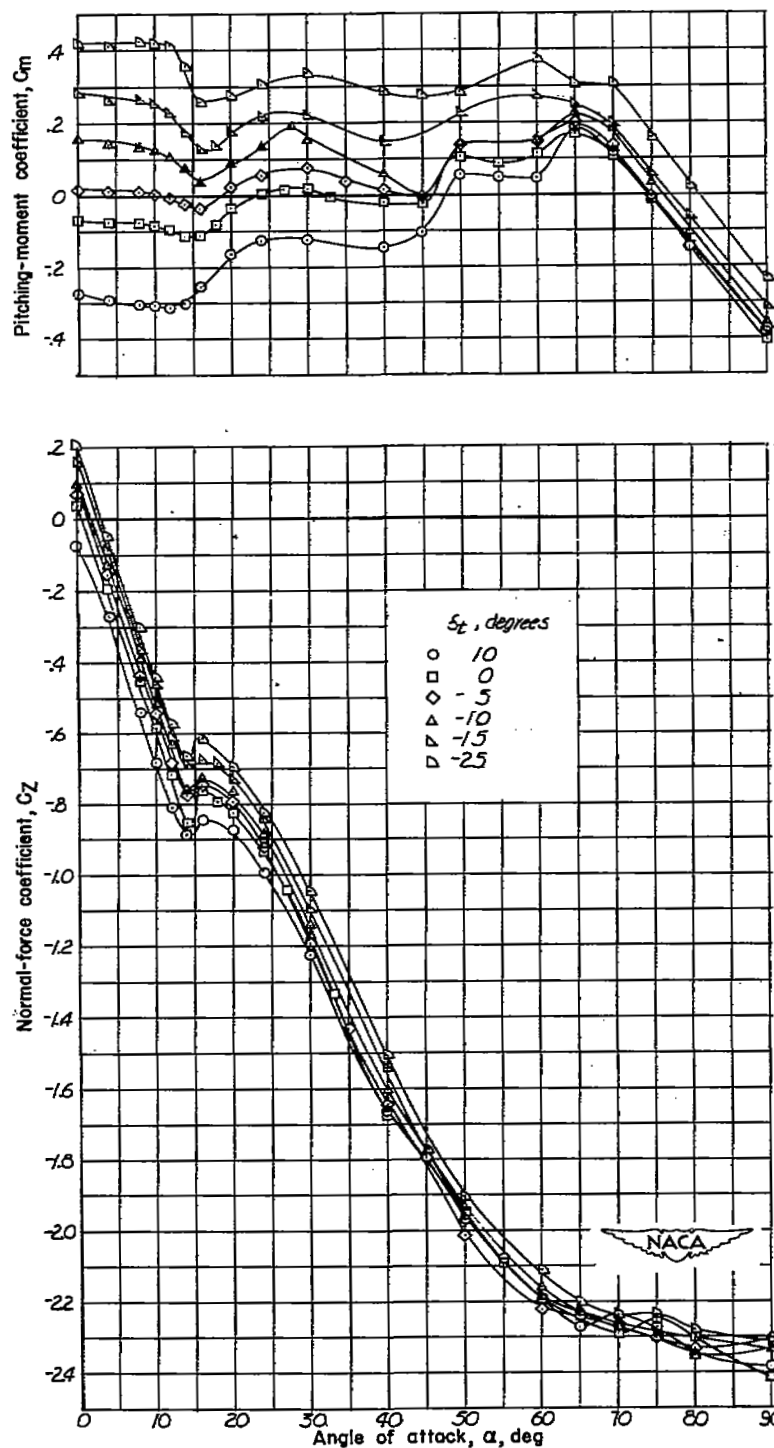


Figure 9.- Effect of horizontal tail setting on the aerodynamic characteristics of the static model tested in the spin tunnel.  $R = 340,000$ .



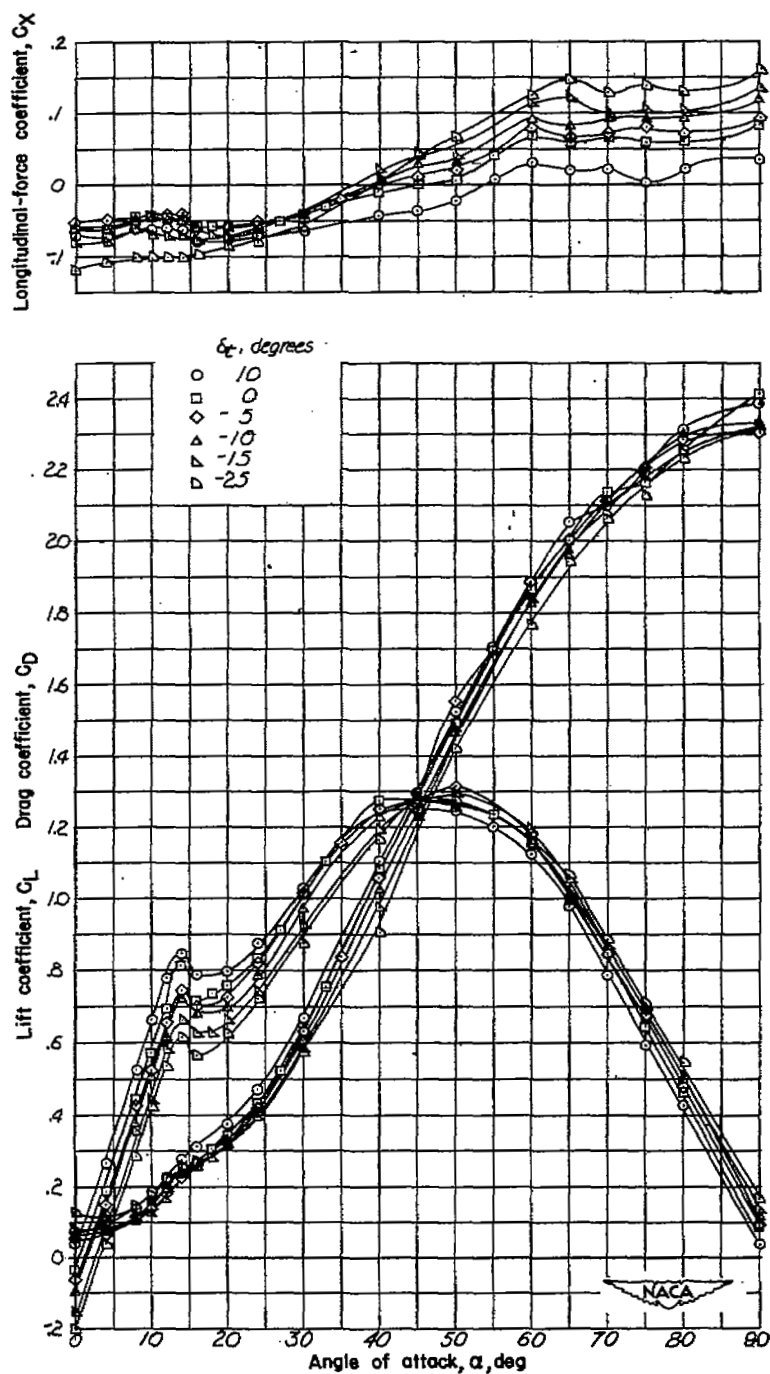


Figure 9.- Concluded.

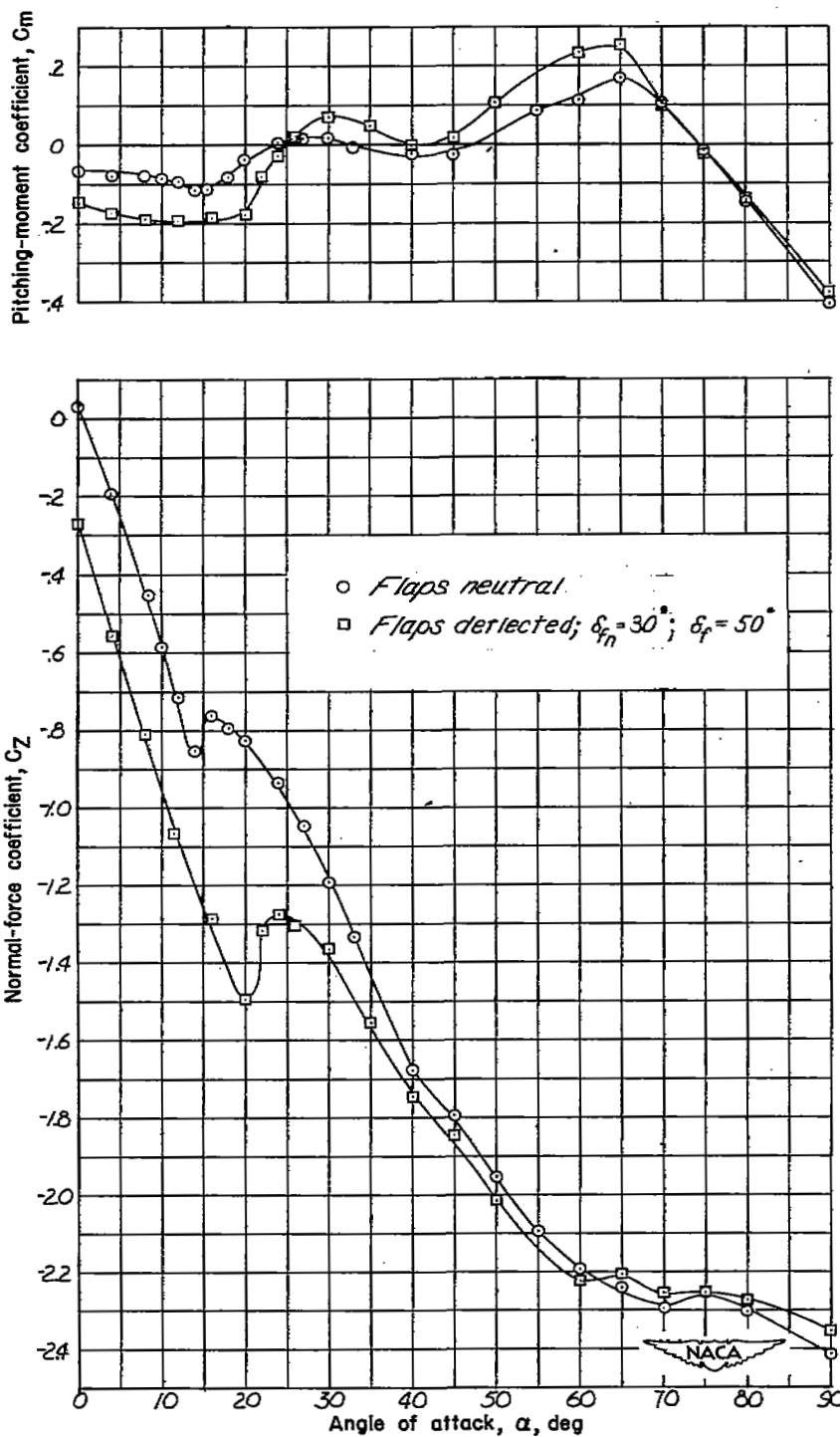


Figure 10.- Effect of flap deflection on the aerodynamic characteristics of the static model tested in the spin tunnel.  $R = 340,000$ ;  $\delta_t = 0^\circ$ .

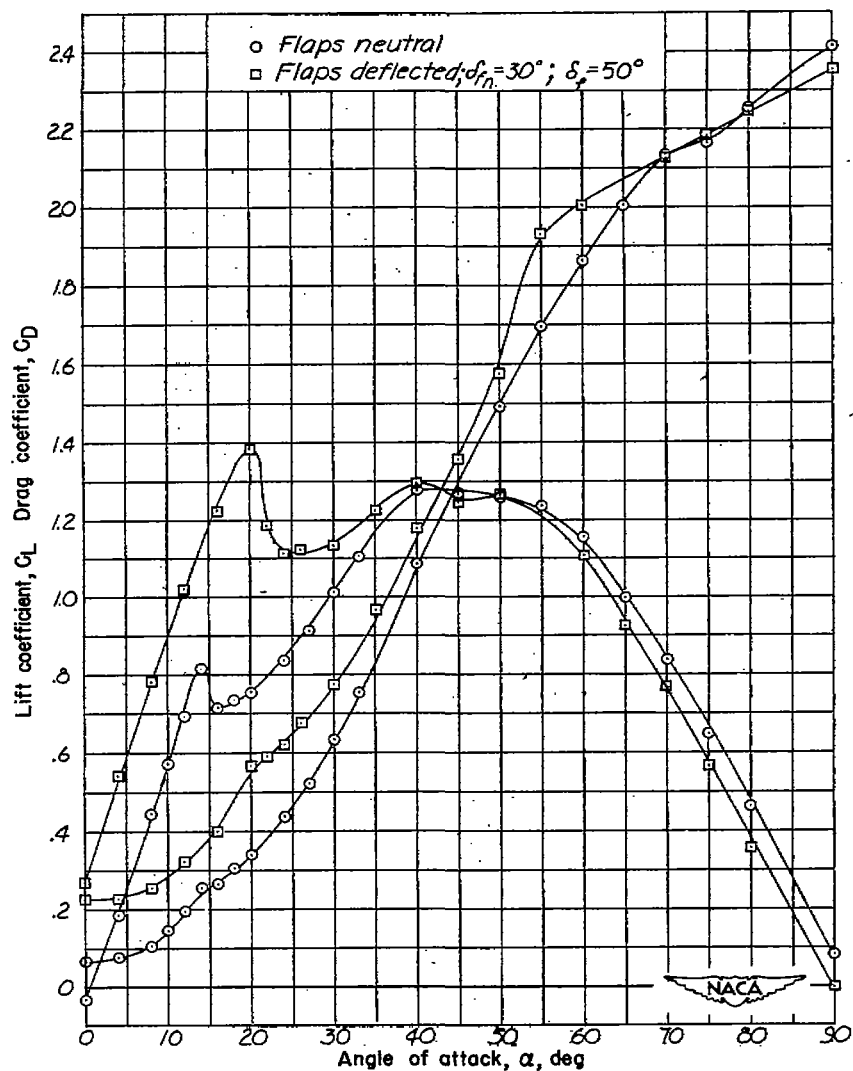
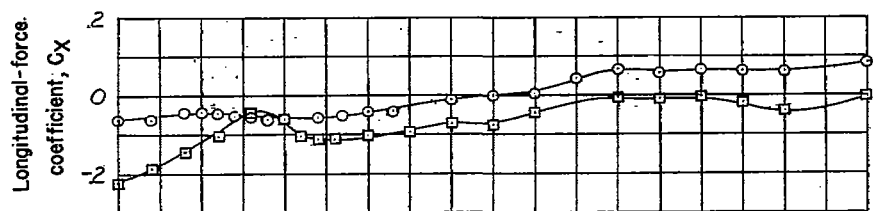


Figure 10.- Concluded.

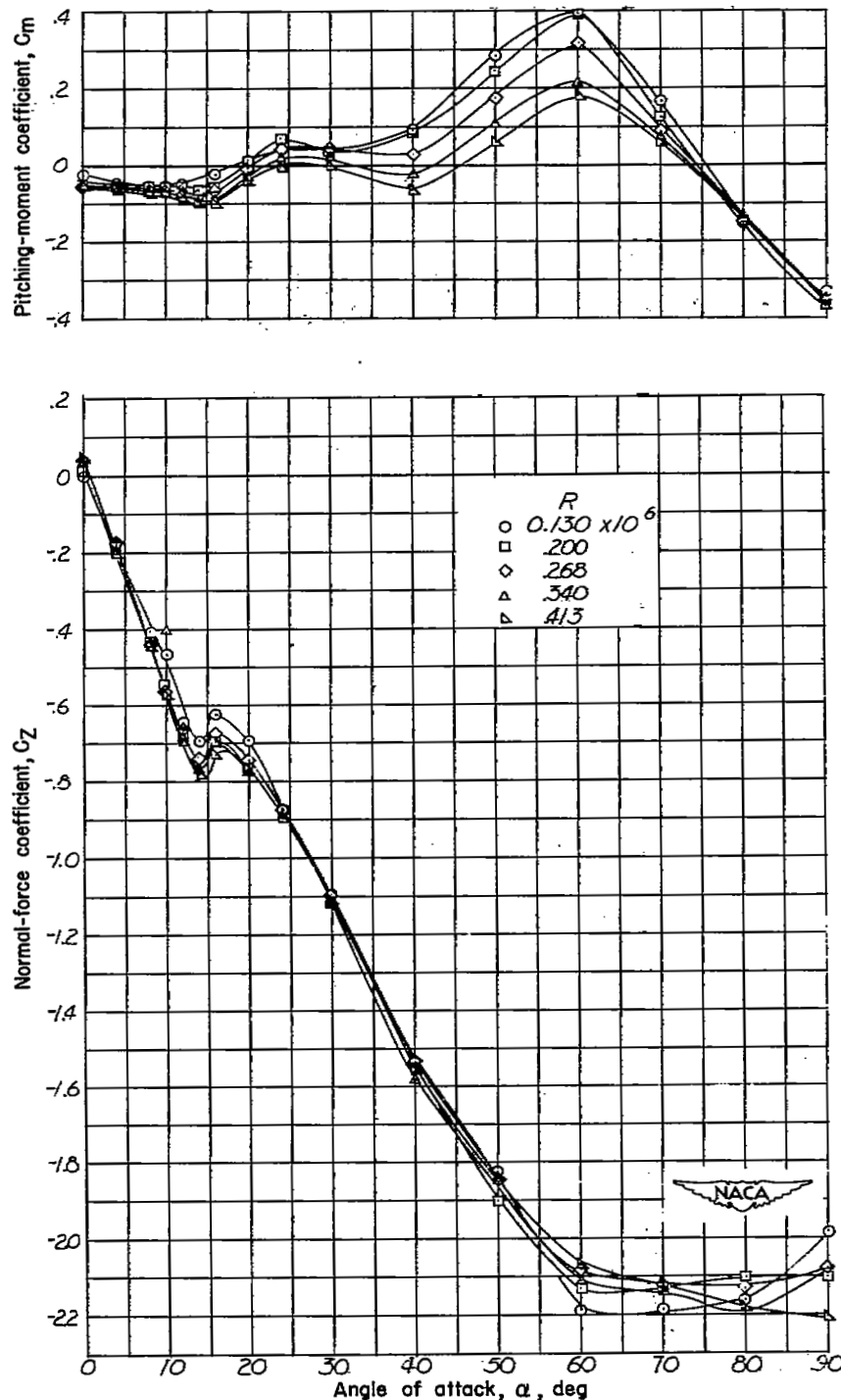


Figure 11.- Effect of Reynolds number on the aerodynamic characteristics of the static model tested in the spin tunnel.  $\delta_t = 0^\circ$ .

~~CONFIDENTIAL~~  
 SECURITY INFORMATION

NACA RM L50L19

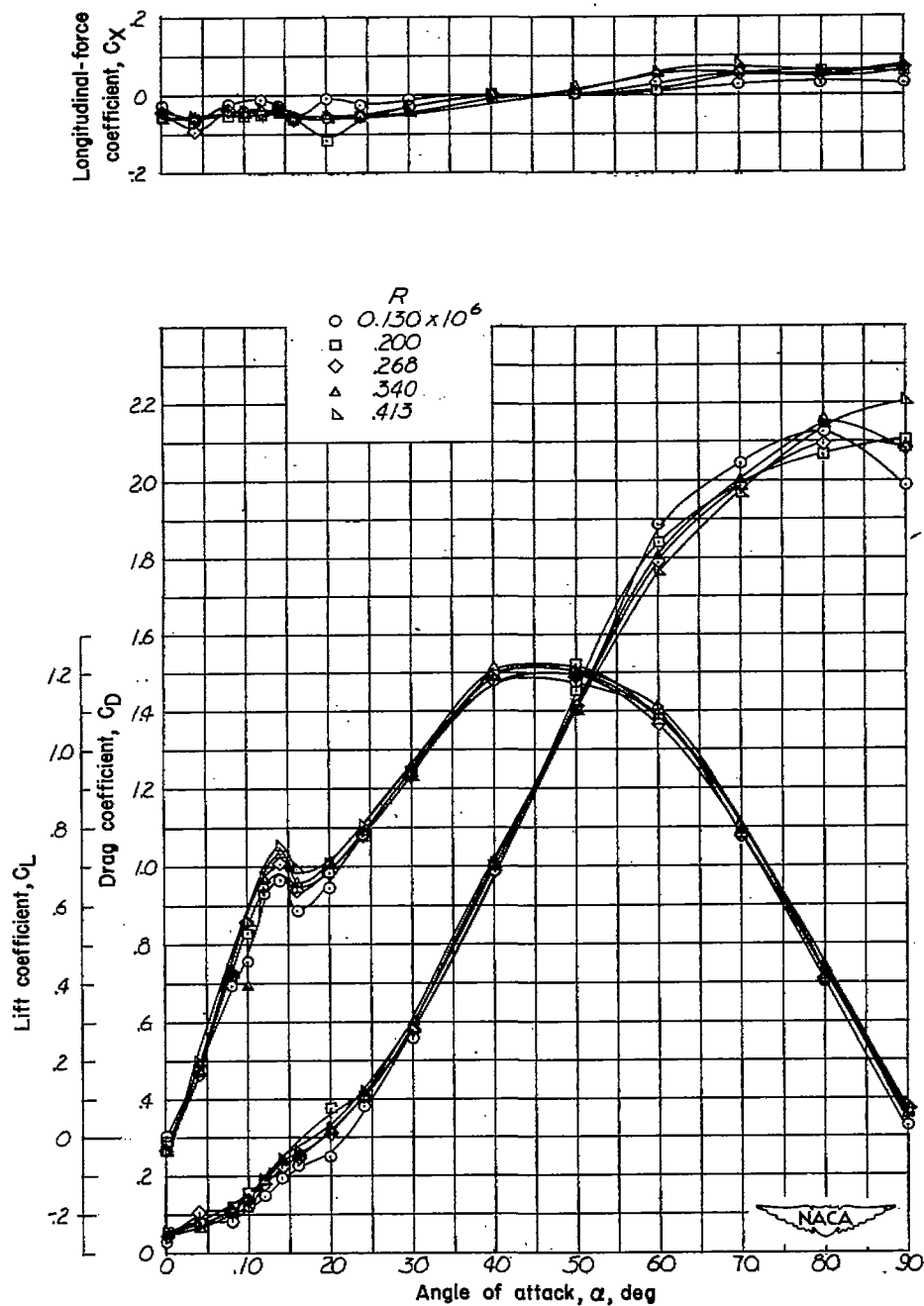
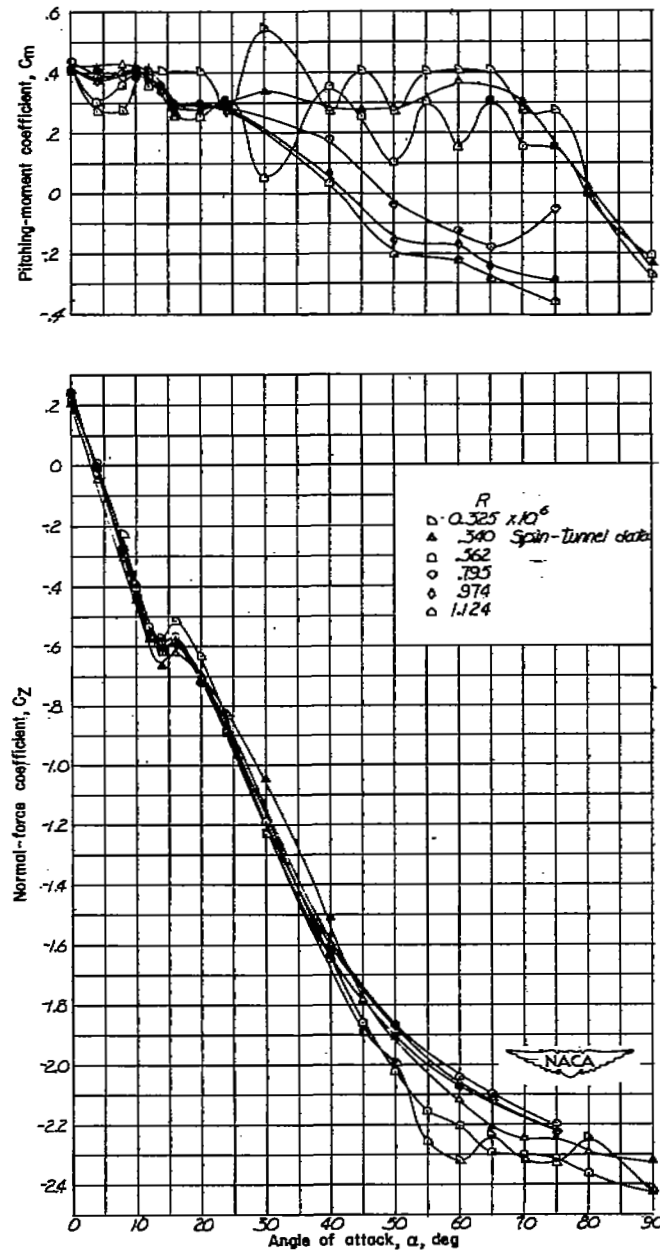


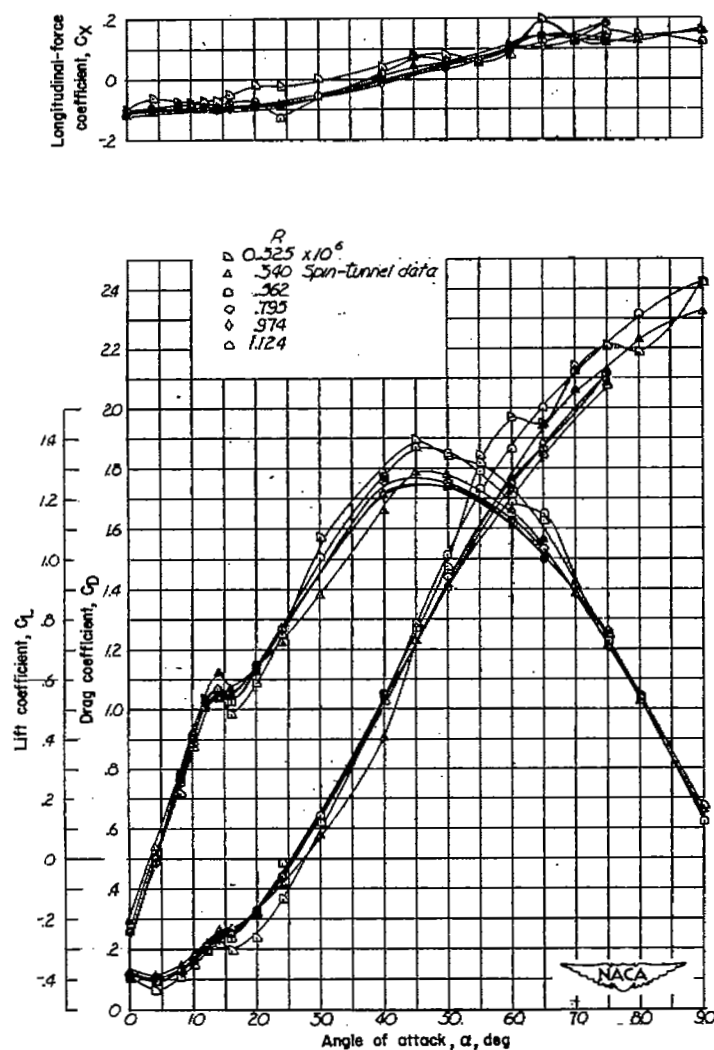
Figure 11.- Concluded.

~~CONFIDENTIAL~~  
 SECURITY INFORMATION



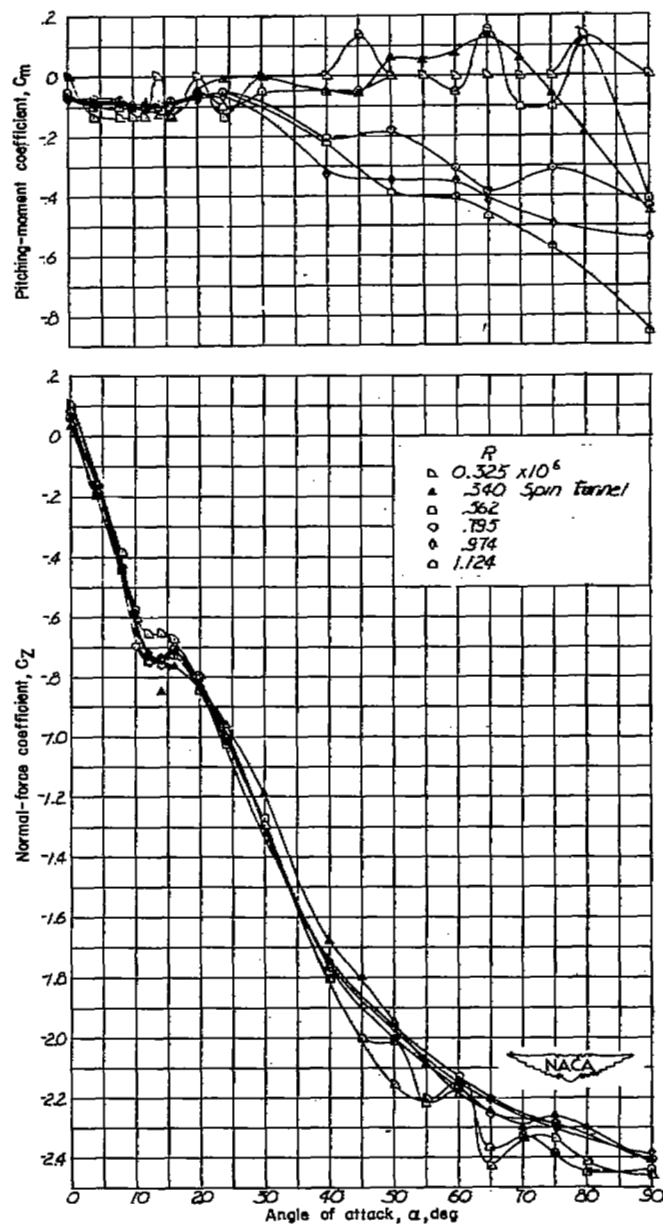
(a)  $\delta_t = -25^\circ$ .

Figure 12.- Effect of Reynolds number on the aerodynamic characteristics of the static model tested in the Langley 300 MPH 7- by 10-foot tunnel.



(a) Concluded.

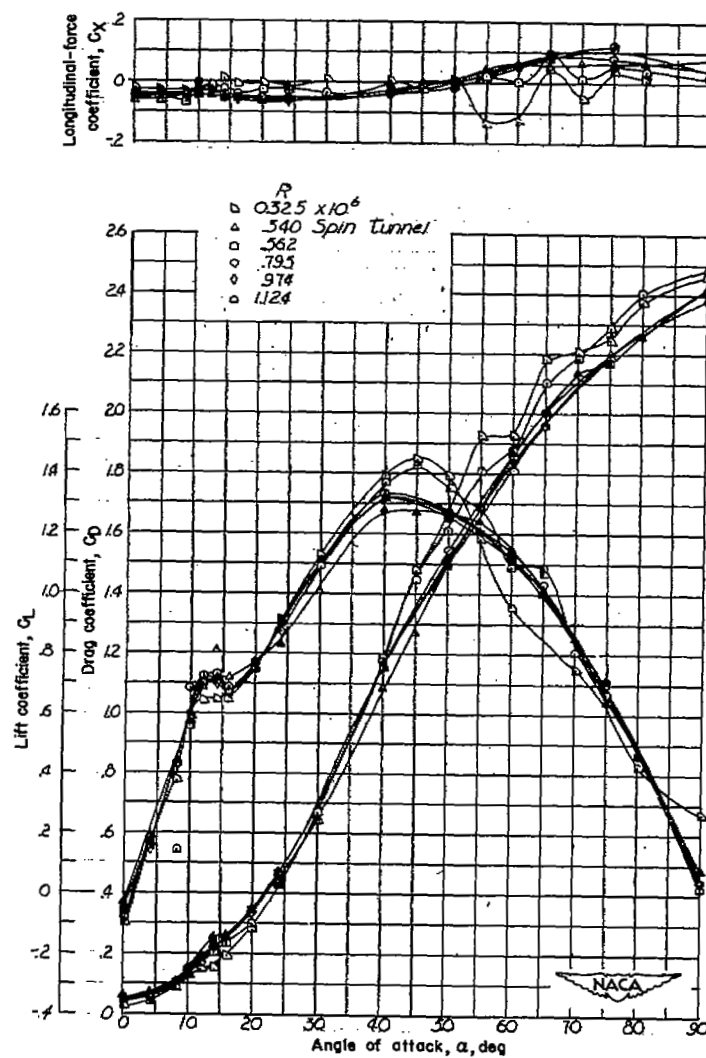
Figure 12.- Continued.



(b)  $\delta_t = 0^\circ$ .

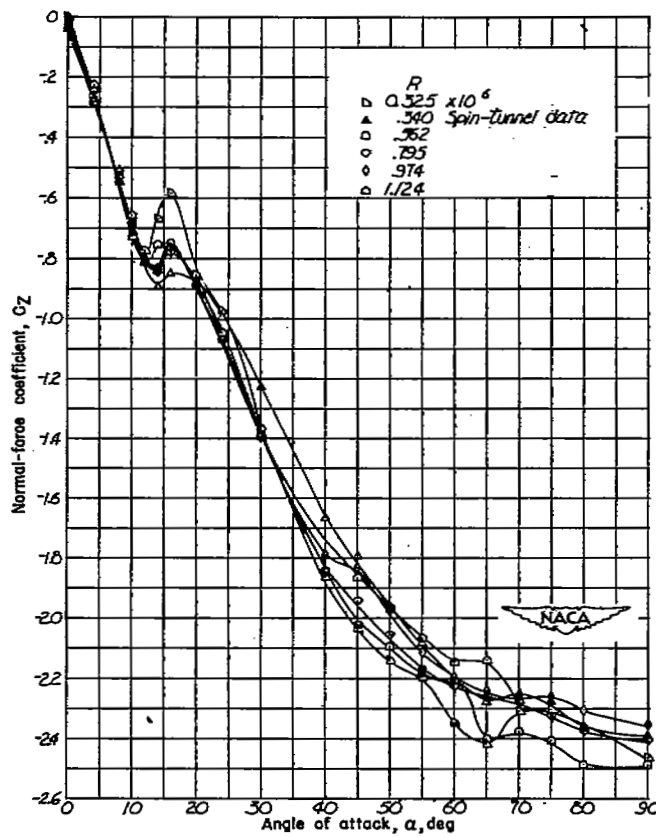
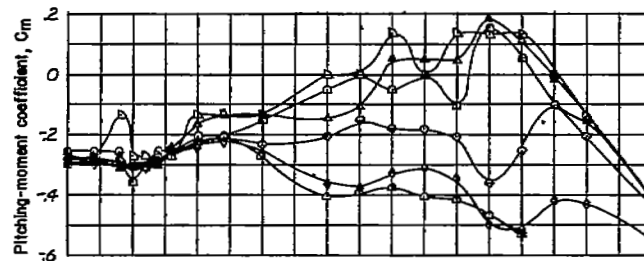
Figure 12.- Continued.





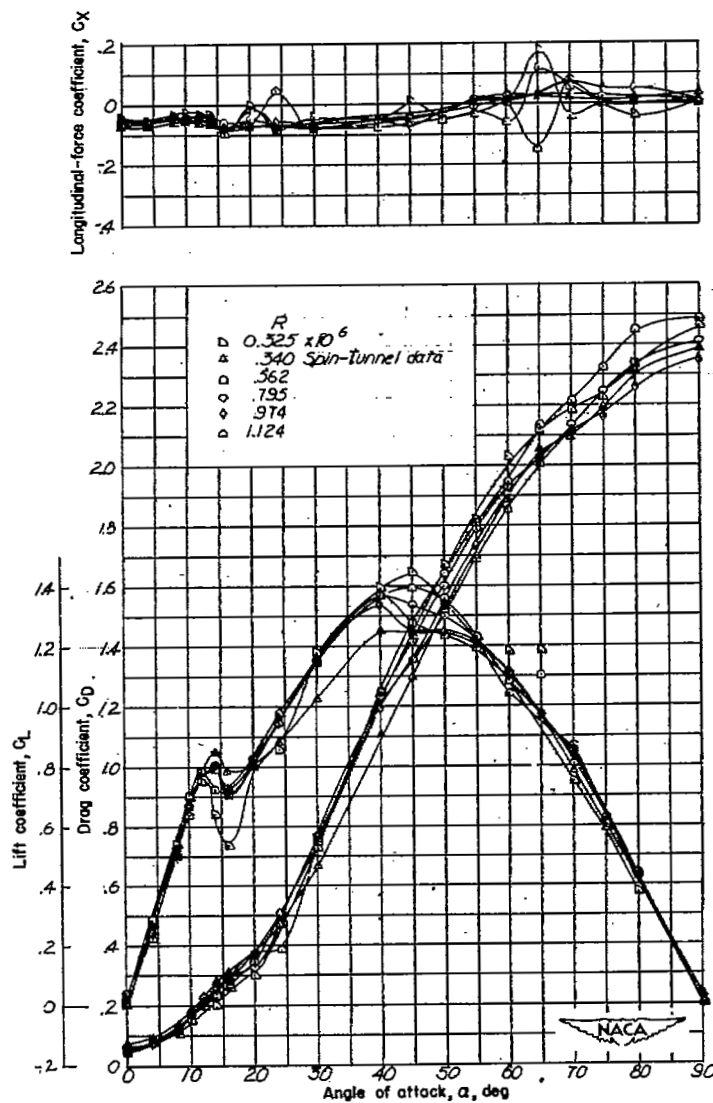
(b) Concluded.

Figure 12.- Continued.



(c)  $\delta_t = 10^\circ$ .

Figure 12.- Continued.



(c) Concluded.

Figure 12.- Concluded.

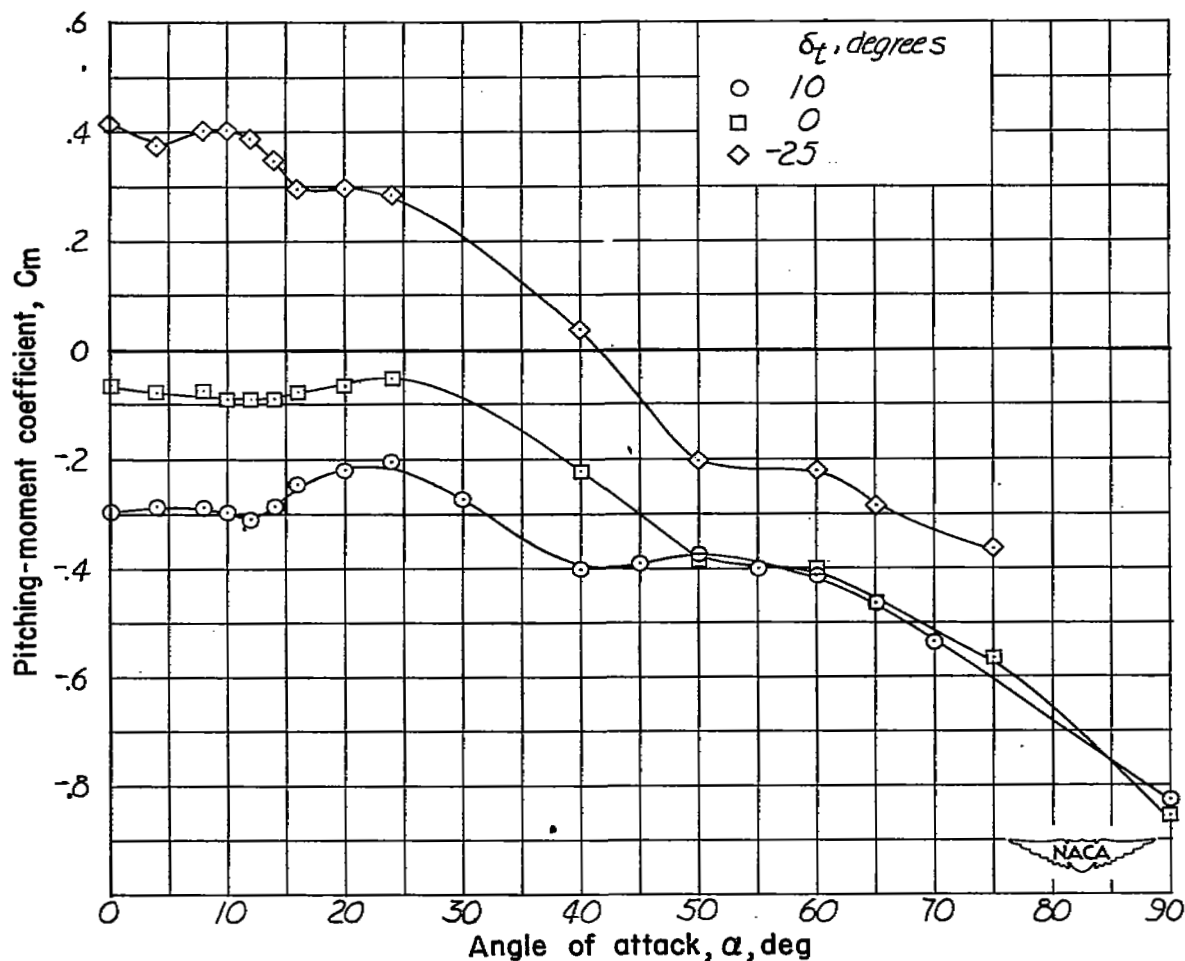


Figure 13.- Effect of horizontal tail deflection on the aerodynamic characteristics of the static model tested in the Langley 300 MPH 7- by 10-foot tunnel.  $R = 1,124,000$ .

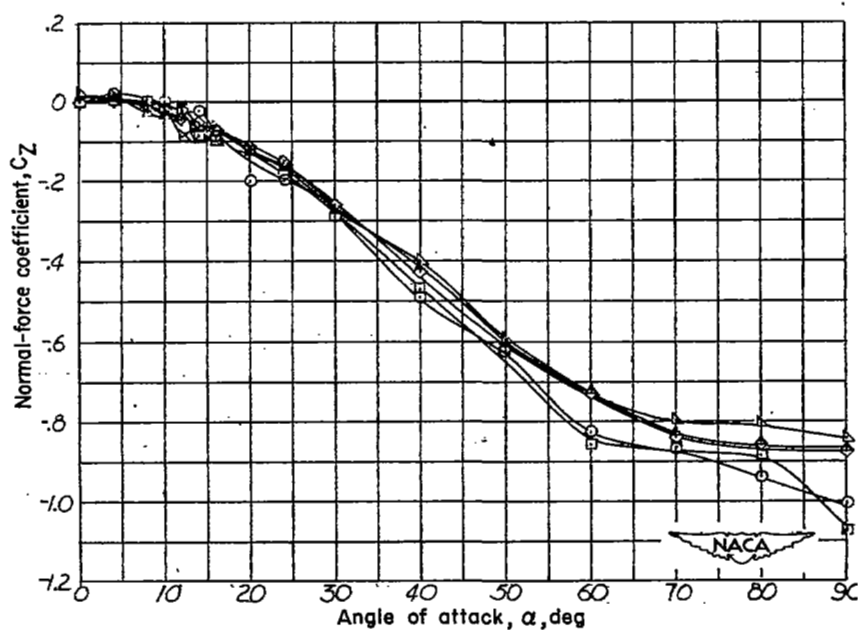
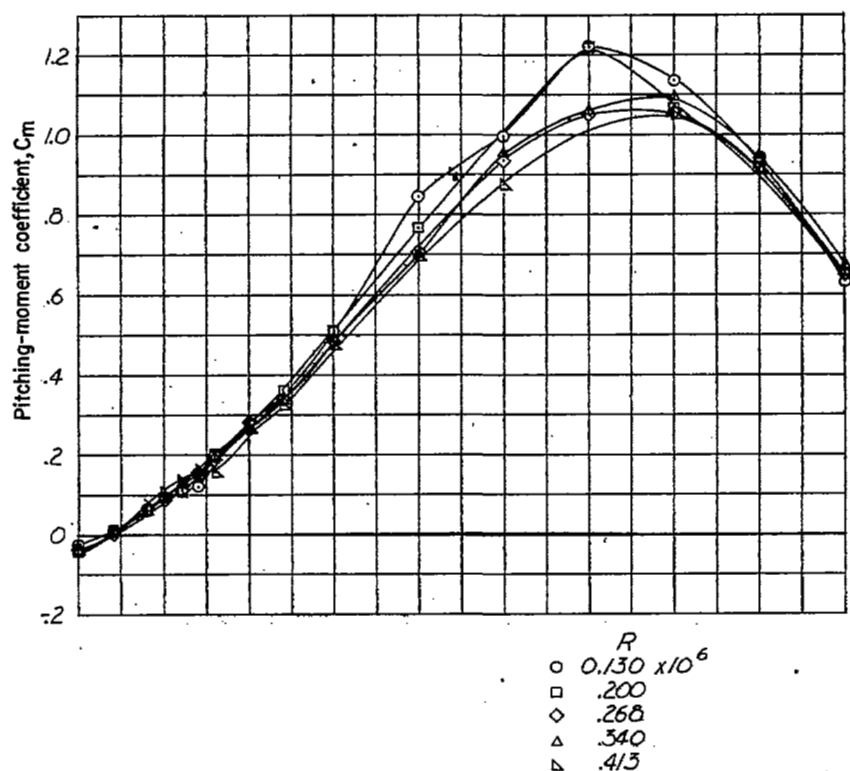


Figure 14.- Effect of Reynolds number on the aerodynamic characteristics of the fuselage alone of the static model tested in the spin tunnel.

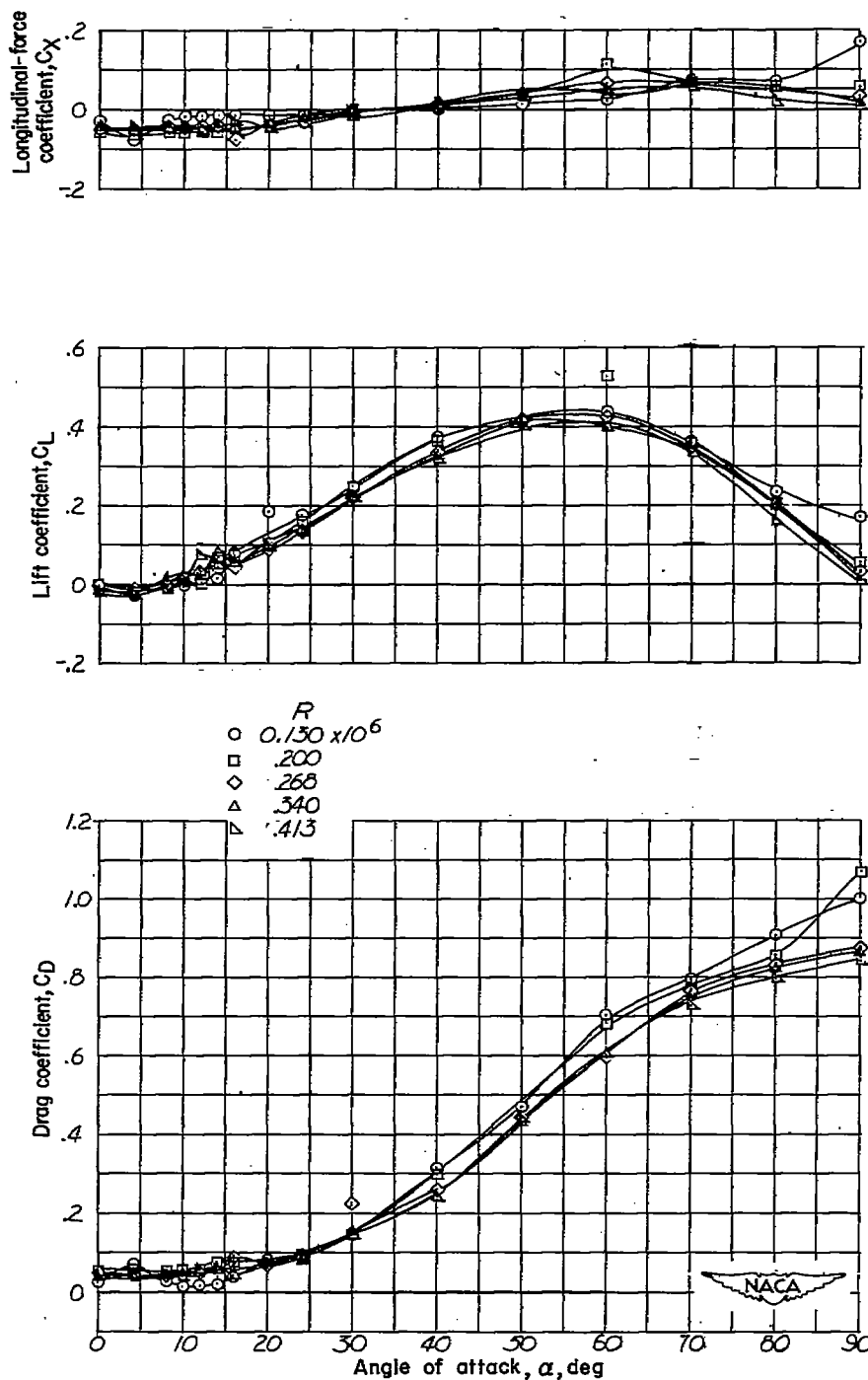


Figure 14.- Concluded.

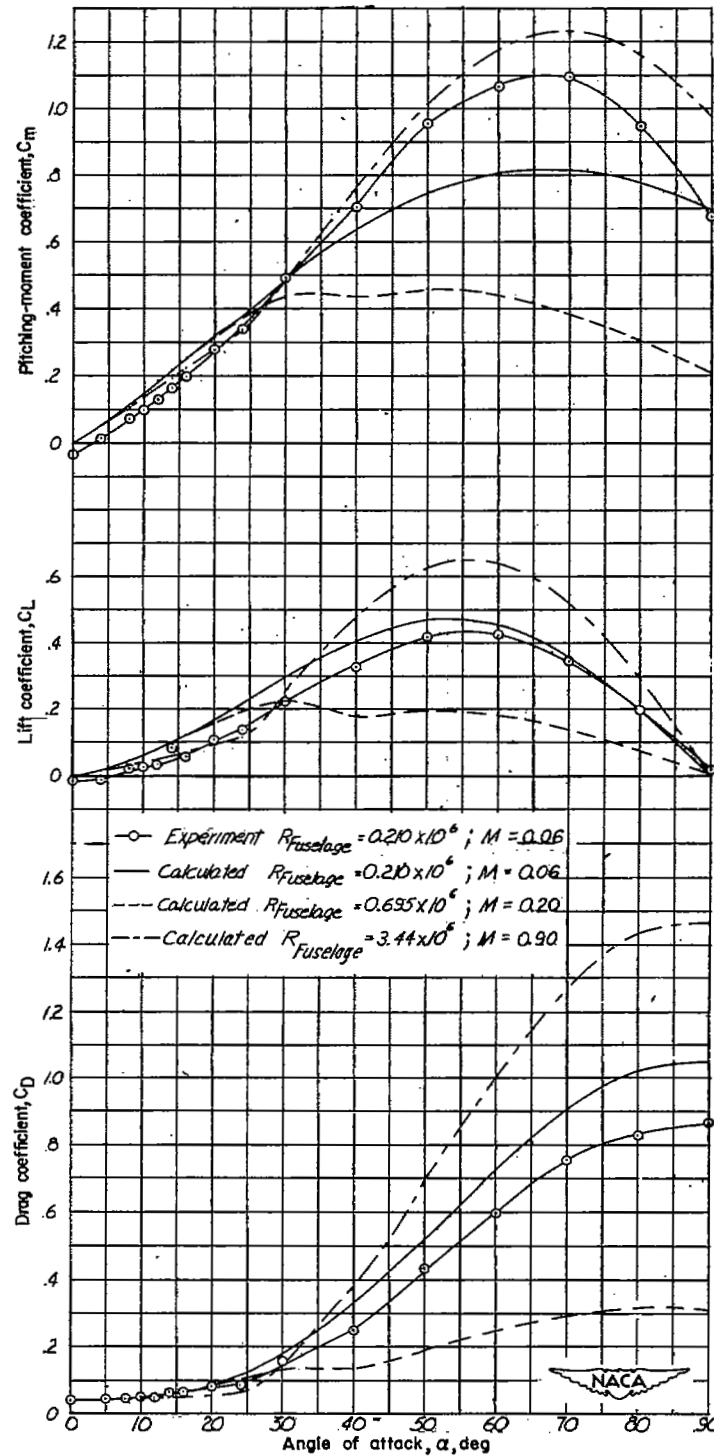


Figure 15.- Comparison between experimental and calculated results for the fuselage alone.

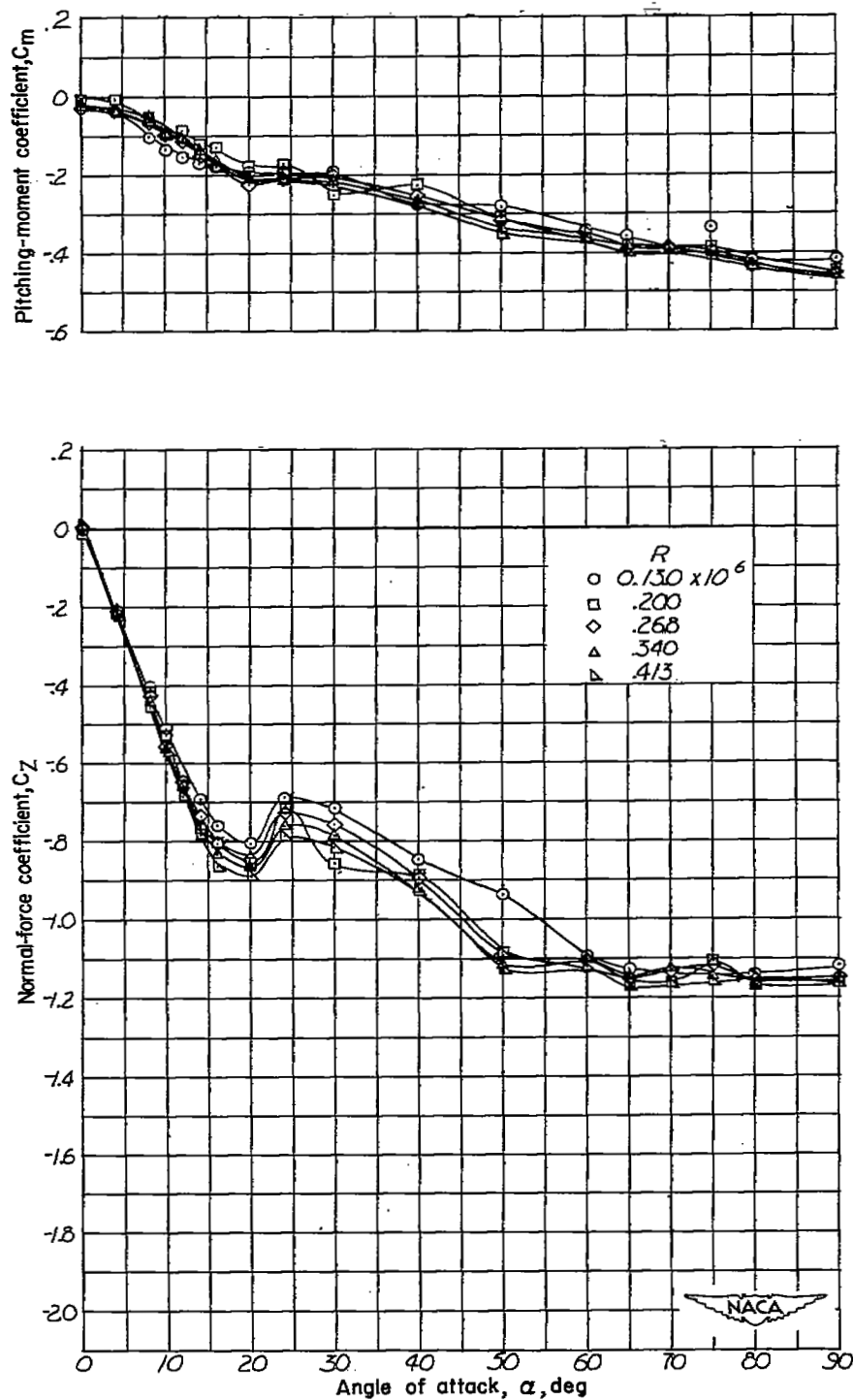


Figure 16.- Effect of Reynolds number on the aerodynamic characteristics of the wing alone of the static model tested in the spin tunnel.



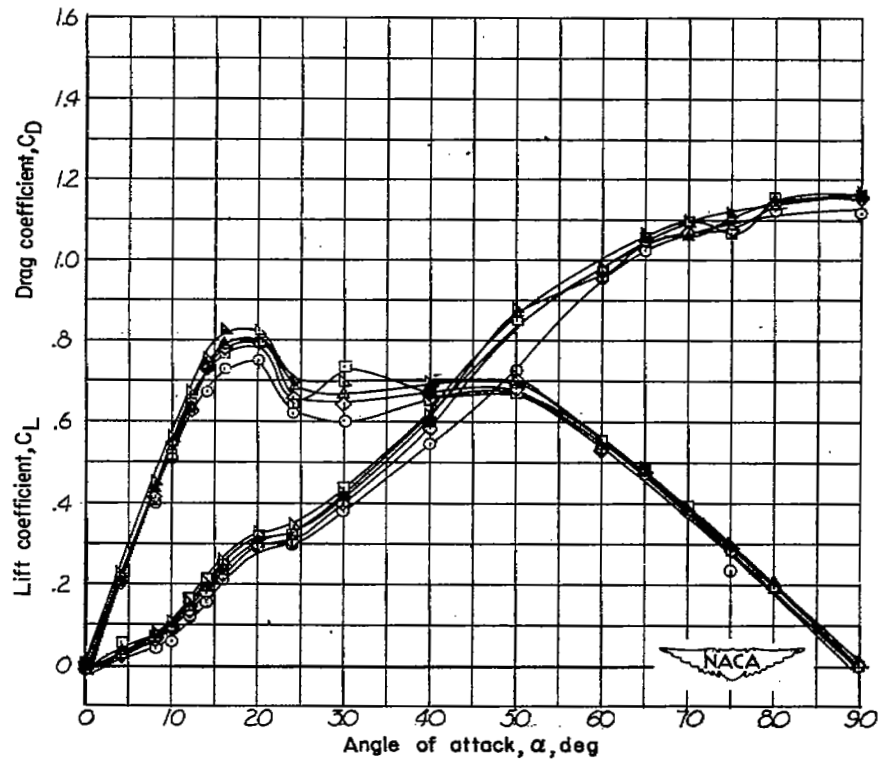
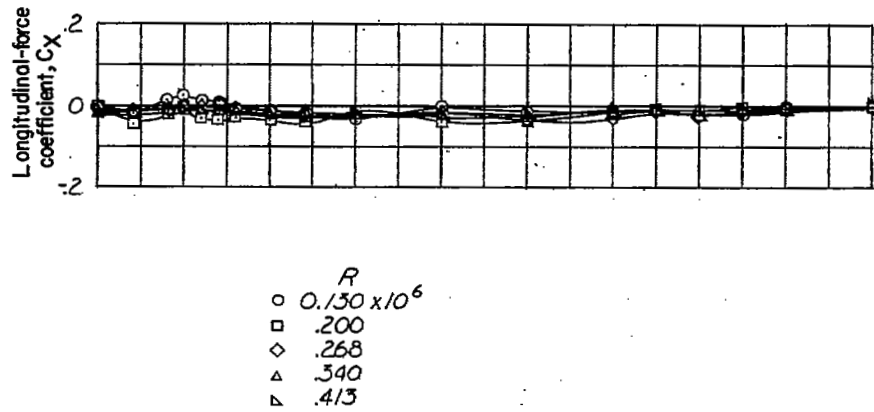


Figure 16.- Concluded.

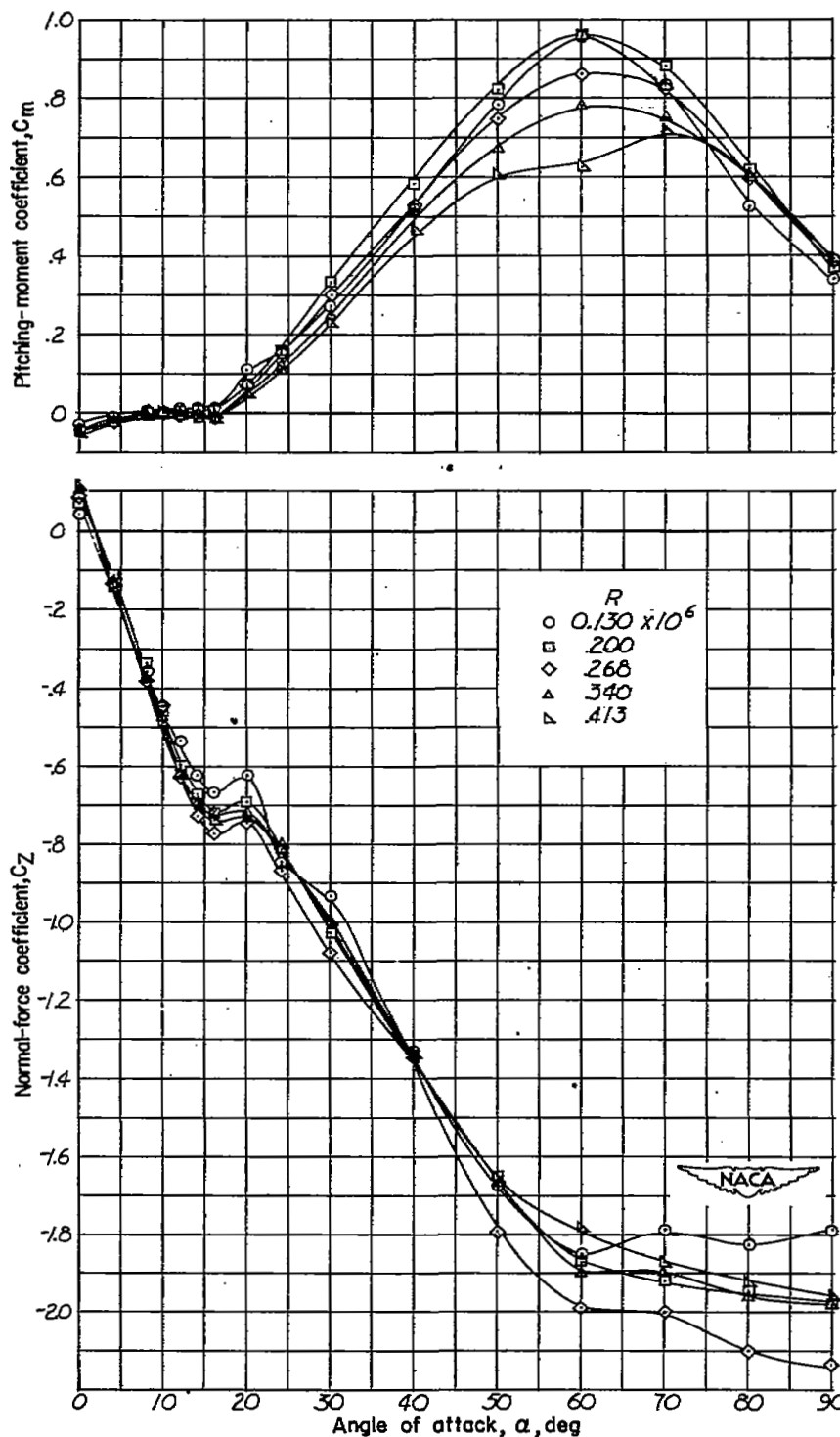


Figure 17.- Effect of Reynolds number on the aerodynamic characteristics of the fuselage plus wing of the static model tested in the spin tunnel.

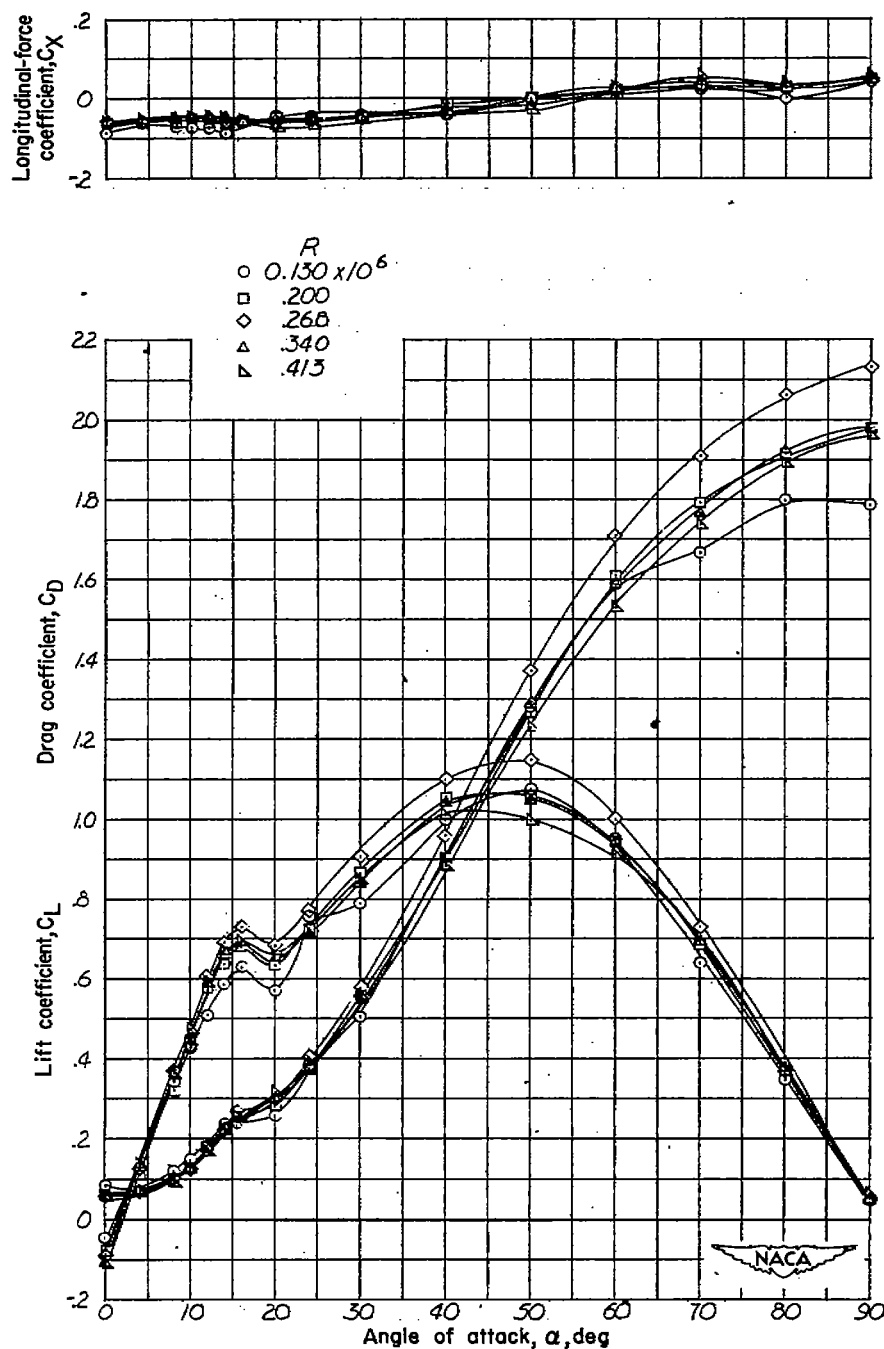


Figure 17.- Concluded.

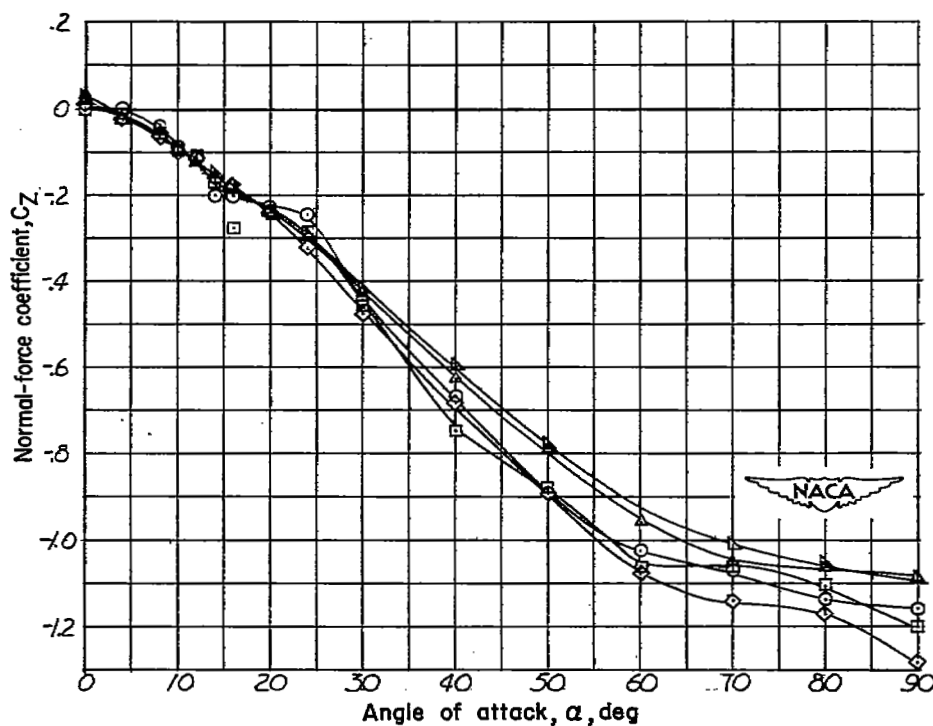
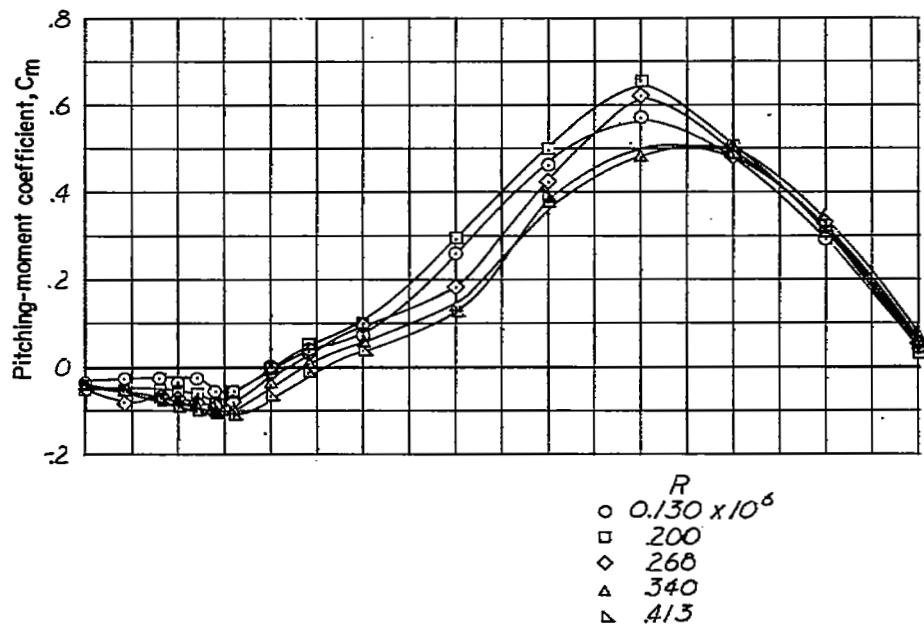


Figure 18.- Effect of Reynolds number on the aerodynamic characteristics of the fuselage plus horizontal tail of the static model tested in the spin tunnel.  $\delta_t = 0^\circ$ .

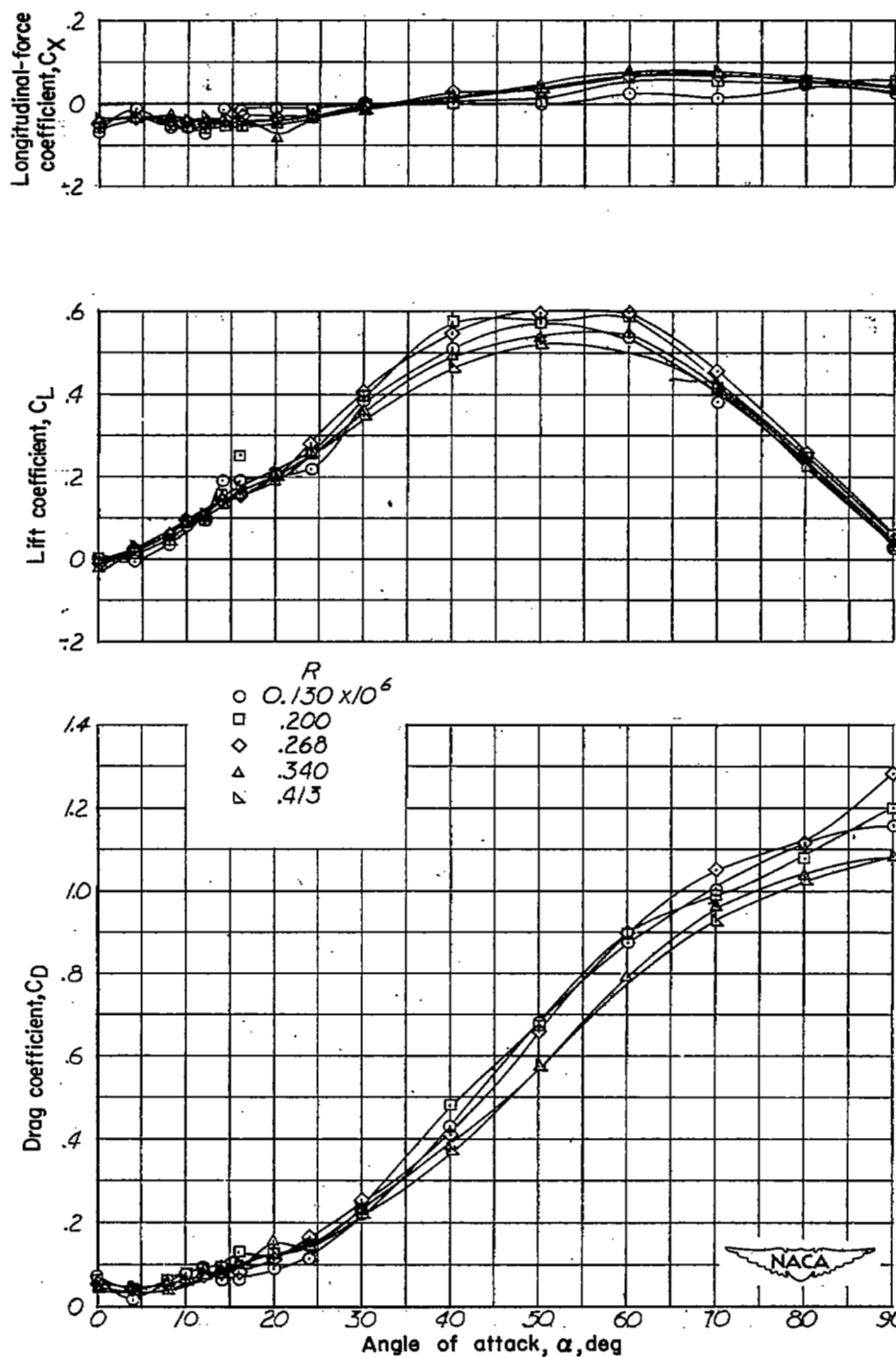


Figure 18.- Concluded.